Available online at www.sciencedirect.com
SCIENCE DIRECT
ELSEVIER
Tectonophysics 416 (2006) 245–277
TECTONOPHYSICS
www.elsevier.com/locate/tecto

Global 1° × 1° thermal model TC1 for the continental lithosphere: Implications for lithosphere secular evolution

Irina M. Artemieva

Geological Institute, Copenhagen University, Denmark

Accepted 28 November 2005
Available online 9 February 2006

Abstract

This paper reports a new 1° × 1° global thermal model for the continental lithosphere (TC1). Geotherms for continental terranes of different ages (>3.6 Ga to present) constrained by reliable data on borehole heat flow measurements (Artemieva, I.M., Mooney, W.D. 2001. Thermal structure and evolution of Precambrian lithosphere: a global study. J. Geophys. Res 106, 16387–16414.), are statistically analyzed as a function of age and are used to estimate lithospheric temperatures in continental regions with no or low-quality heat flow data (ca. 60% of the continents). These data are supplemented by cratonic geotherms based on electromagnetic and xenolith data; the latter indicate the existence of Archean cratons with two characteristic thicknesses, ca. 200 and >250 km. A map of tectono-thermal ages of lithospheric terranes complied for the continents on a 1° × 1° grid and combined with the statistical age relationship of continental geotherms ($z = 0.04 * t + 93.6$, where z is lithospheric thermal thickness in km and t is age in Ma) formed the basis for a new global thermal model of the continental lithosphere (TC1). The TC1 model is presented by a set of maps, which show significant thermal heterogeneity within continental upper mantle, with the strongest lateral temperature variations (as large as 800 °C) in the shallow mantle. A map of the depth to a 550 °C isotherm (Curie isotherm for magnetite) in continental upper mantle is presented as a proxy to the thickness of the magnetic crust; the same map provides a rough estimate of elastic thickness of old (>200 Ma) continental lithosphere, in which flexural rigidity is dominated by olivine rheology of the mantle.

Statistical analysis of continental geotherms reveals that thick (>250 km) lithosphere is restricted solely to young Archean terranes (3.0–2.6 Ga), while in old Archean cratons (3.6–3.0 Ga) lithospheric roots do not extend deeper than 200–220 km. It is proposed that the former were formed by tectonic stacking and underplating during paleocollision of continental nuclei; it is likely that such exceptionally thick lithospheric roots have a limited lateral extent and are restricted to paleoterrane boundaries. This conclusion is supported by an analysis of the growth rate of the lithosphere since the Archean, which does not reveal a peak in lithospheric volume at 2.7–2.6 Ga as expected from growth curves for juvenile crust.

A pronounced peak in the rate of lithospheric growth (10–18 km^3/year) at 2.1–1.7 Ga (as compared to 5–8 km^3/year in the Archean) well correlates with a peak in the growth of juvenile crust and with a consequent global extraction of massif-type anorthosites. It is proposed that large-scale variations in lithospheric thickness at cratonic margins and at paleoterrane boundaries controlled anorogenic magmatism. In particular, mid-Proterozoic anorogenic magmatism at the cratonic margins was caused by edge-driven convection triggered by a fast growth of the lithospheric mantle at 2.1–1.7 Ga. Belts of anorogenic magmatism within cratonic interiors can be caused by a deflection of mantle heat by a locally thickened lithosphere at paleosutures and, thus, can be surface manifestations of exceptionally thick lithospheric roots. The present volume of continental lithosphere as estimated from the new global map of lithospheric thermal thickness is 27.8 (± 7.0) × 10^9 km^3 (excluding submerged terranes

E-mail address: Irina@geol.ku.dk.

0040-1951/$ - see front matter
doi:10.1016/j.tecto.2005.11.022

with continental crust); preserved continental crust comprises ca. 7.7×10^9 km^3. About 50% of the present continental lithosphere existed by 1.8 Ga.

Keywords: Mantle temperature; Lithosphere thickness; Anorthosites; Xenolith geotherms; Electrical conductivity; Growth rate

1. Introduction

Laboratory measurements on upper mantle rocks and rock-forming minerals reveal strong dependence of seismic velocities and electrical conductivity on temperature (Kampfmann and Berckhemer, 1985; Jackson, 2000; Constable et al., 1992). Although recent high-resolution global and regional seismic tomography and electromagnetic surveys image strong lateral and vertical heterogeneities within the continental upper mantle (e.g., Freybourger et al., 2001; Jones et al., 2003), no reliable interpretations of their origin (thermal, structural, or compositional) are possible in the absence of data on upper mantle temperatures. The contribution of thermal versus compositional variations to observed geophysical anomalies remains controversial. Forte et al. (1994) conclude that much of seismic velocity variations in the mantle can be attributed to temperature variations. On the other side, Poupinet et al. (2003) found that P-wave travel time delays correlate well with geological ages and concluded that temperature variations alone cannot explain short-wavelength offsets in P-vertical travel times, but require mineralogical differences within the lithosphere. Griffin et al. (1998a) argue that compositional anomalies can account for at least 50% of the velocity anomalies observed in seismic tomography models. This conclusion agrees with the results of a global analysis of correlations between seismic and thermal anomalies, which indicate that in the upper 150 km of the continental mantle temperature variations alone are sufficient to explain seismic *V*s only in ca. 50% of continental regions; in other continental regions temperature variations can account for not more than 50% of the amplitude of seismic velocity anomalies (Artemieva et al., 2004).

Clearly, estimates of upper mantle temperatures from seismic tomography (e.g., Furlong et al., 1995; Sobolev et al., 1996; Godey et al., 2004) or electrical conductivity models (e.g., Dobson and Brodholt, 2000; Ledo and Jones, 2005) cannot be used to assess the relative contributions of thermal and compositional variations to geophysical anomalies, because such inversions require certain assumptions on mantle composition, fluid regime, and the amount of melt, while anisotropy can also significantly affect the results. A more advanced approach has been recently proposed by Shapiro and Ritzwoller (2004a), who assimilated heat flow data into seismic inversion and used seismic tomography data to estimate mantle temperatures beneath Antarctica. Alternatively, xenolith data can be used to estimate mantle geotherms. However, the number of localities with mantle-derived peridotites is very limited and their areal distribution is much more scarce than heat flow measurements (Fig. 1).

The present study reports a new consistent global thermal model TC1 for the continental upper mantle constrained primarily by heat flow data and thus suitable for interpretations of seismic, gravity, or electromagnetic models in terms of thermal versus non-thermal anomalies. A thermal model for stable continental lithosphere constrained by reliable surface heat flow (Artemieva and Mooney, 2001) provides the basis for the present study. However, because the coverage of borehole measurements is uneven and sparse in many regions (Fig. 1), heat flow data permit constraints on lithospheric geotherms for only about 40% of the continents. In particular, high-quality heat flow measurements are absent for ~80% of South America, ~70% of Africa, large areas in Asia, all of Antarctica, most of Greenland, the Arctic regions of North America, and the Russian Far East. Nevertheless, a number of heat flow measurements in continental terranes of different geological ages permits statistically significant analysis of lithospheric geotherms for different tectonic settings allowing expansion of the previous thermal model (Artemieva and Mooney, 2001) to all continental areas (excluding submerged terranes with continental crust such as oceanic plateaus and shelves). Xenolith P–T arrays as well as data on electrical conductivity of the upper mantle have been compiled for different cratonic settings and compared with lithospheric geotherms constrained by surface heat flow. For tectonically active regions with transient thermal regimes, lithospheric temperatures are based primarily on xenolith geotherms.

A compilation of ages of the continental crust averaged on a $1°\times1°$ grid formed the basis of the

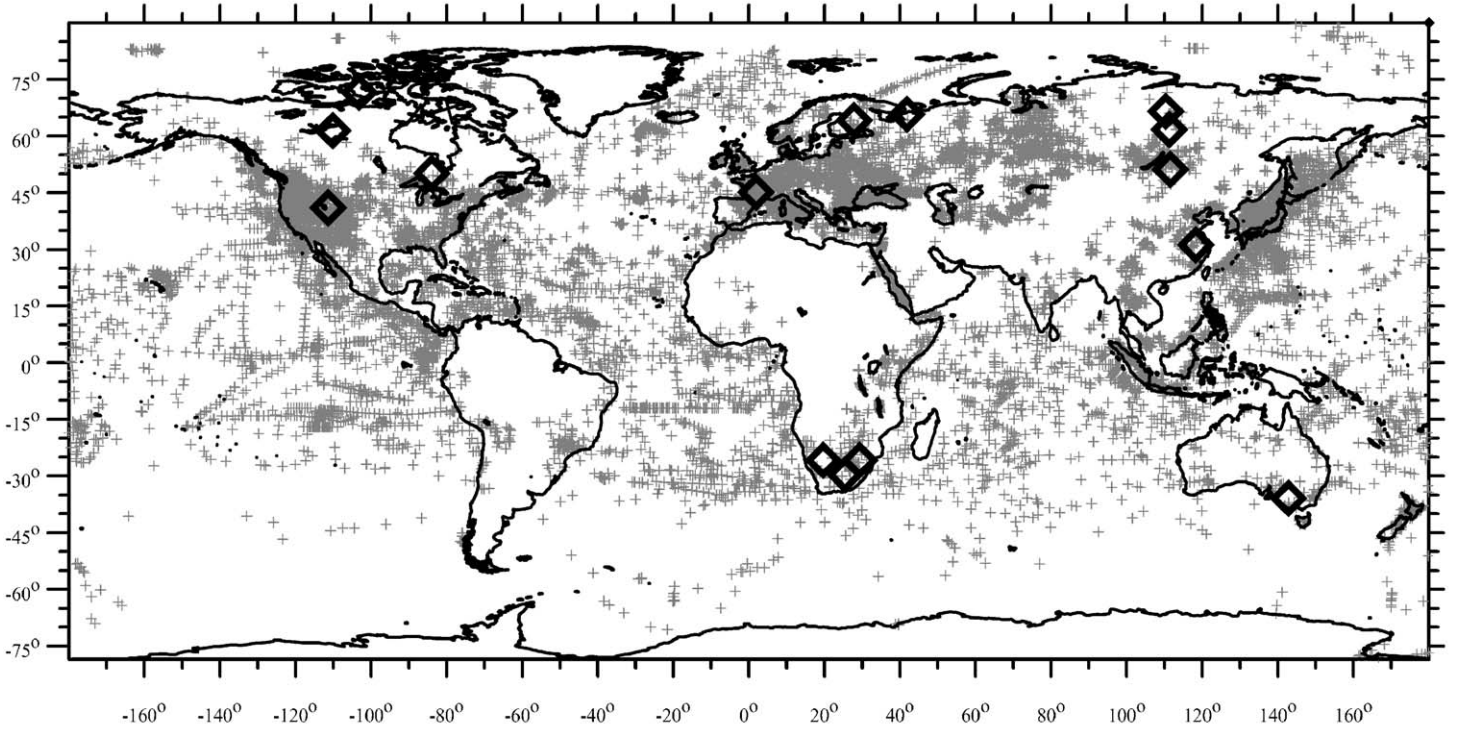

Fig. 1. Global heat flow data coverage (updated after Pollack et al., 1993). Crosses—sites of borehole heat flow measurements; diamonds—locations of mantle xenoliths discussed in the text.

Table 1
Geologic and tectonic ages and lithospheric thermal thickness for major Precambrian provinces

Precambrian cratons	Basement age (Ga)*	Cratonization age (Ga)	Major tectonic events (Ga)	Thermal thickness (km) (uncertainty ca. 25%)
Australian craton				
Pilbara craton	**3.5–3.0**	3.0	2.0–1.7, 1.3–1.0	170–230
Yilgarn craton	**3.7–3.4** gneiss and 3.0–2.6 granites (3.7)	2.7–2.6		170–230
Hamersley and Naberru basins	Archean?		**2.8–2.3**	No data
Gawler carton	**2.7–2.6**	1.5	1.9–1.8, 1.6–1.5	170–190
North Australian craton	**2.1–1.9 (2.5)**	1.85	1.3–1.1	130–200
Central Australian mobile belt	**1.9–1.4**	1.2–1.1	1.8–1.6, 1.5–1.3, 1.1–1.0, 0.9–0.5	140–160
South American craton				
Amazonian craton (Guyana Shield)	**3.4 and 2.9–2.6** (3.5)	2.8–2.6	2.2–2.1, 1.85–1.55	No data
Mobile belts of Amazonian craton	**2.2–1.8**			No data
Central Brazil shield	**3.0–2.8** (3.2)	2.8–2.6	2.1–1.9, 1.6–1.1, 0.7–0.5	No data
Mobile belts of Central Brazil shield	Archean–early Proterozoic		**1.4**	No data
Atlantic shield (Sao Francisco craton)	**3.2** (3.4)	2.8–2.6	2.1–1.9, 0.6	190–200
Marginal belts of Atlantic shield	**1.1**		0.7–0.5	110–160
Rio Apa craton	**1.6–1.0** (2.1)			No data
Indian craton				
Dharwar craton	**3.1–3.0**	2.6–2.5		180–200
Southern Granulite terrane	**3.3–3.0** (3.4)	2.6–2.5	2.1–2.0, 1.6–1.5, 0.9	180–230
Singhbhum craton	**3.4**	2.6–2.5	2.1	160–200
Aravalli craton	**3.4**	2.6–2.5	2.5–2.0, 1.8–1.5	160–200
Bhandara (Bastar) craton	**3.5–3.3**		2.2, 1.0	180–200
Cuddapah Basin	**2.0–1.5**		1.5–1.0	140–160
Narmada–Son rift system			**0.6–0.5**	80–110
Siberian craton				
Aldan shield and Stanovoy Ridge	**3.4–3.2**	3.1–2.9, 2.6–2.5	Partly at 2.0–1.8	140–190
Kolyma–Omolon and Okhotsk median massifs	**3.4**	?	1.6–0.5	No data
Anabar shield	**2.9–2.7** (3.2)	2.6–2.5	1.9, partly at 0.9–0.5	190–350
Main Siberian craton	Mainly Ar (ca. 75%), extensively reworked at **1.95–1.8 Ga** by epicratonic rifting	2.6–2.5	1.4–1.1, 0.8–0.5; Mz (Viluy basin)	150–350 (120–140 Viluy basin)
Pericratonic mobile belts	**3.2–2.5**		2.5, 1.9, 0.6	250–350
East-European craton				
Ukrainian shield and Voronezh massif	**3.6–3.0**	3.2, 2.7–2.5	2.3–1.8, 1.4	170–230
Baltic shield (Kola–Karelia and Lapland)	**2.9–2.7** (3.1)	2.7–2.6		200–300
SvecoFennian province	**2.0–1.8**			170–200
SvecoNorwegean province	1.75–1.5, extensively reworked at **1.1–0.9 Ga**		0.6–0.4	150–180
Transscandinavian Belt	1.8–1.6			110–140
East European platfrom	Ar (75%) and ePt (25%). Extensively reworked at **2.2–1.8 Ga** by wide-spread rifting	2.7–2.6	1.6–0.6	170–220
Volga–Urals anteclise	**~3.0**		1.6–0.6	200–220
Central Russia Rift System			**1.3–0.6**	170–200
North American craton				
Wyoming craton	**3.96–3.4,** extensively	?	2.8–2.6, 1.9–1.8, 0.06	130–150

Table 1 (*continued*)

Precambrian cratons	Basement age (Ga)*	Cratonization age (Ga)	Major tectonic events (Ga)	Thermal thickness (km) (uncertainty ca. 25%)
	reworked in Mz–Cz			
North American craton				
Slave craton	**3.96–3.1** gneiss and **3.1–2.6** granites	2.7–2.6	1.0–0.8	One data point (ca. 200 km)
Wopmay Orogen (Bear province)	**1.9–1.8**			140–180
NE Churchill province (Hearne/Rae cratons)	**2.9–2.7** (3.5)	2.7–2.6		No data
W Churchill province (Taltson and Queen Maud blocks)	2.9–2.7, extensively reworked at **1.9–1.8 Ga**	2.7–2.6		No data
Trans-Hudson orogen	**2.0–1.8**			160–200
Superior craton (north-central part)	>**3.35 and 3.0–2.7**	2.7–2.6		175–240
Superior craton (southern part and Ungava craton)	**3.0–2.7** (3.4)	2.7–2.6	1.9–1.8, 1.5–1.0	150–190
Nutak and Nain cratons (Labrador)	**3.9–3.4**		3.3–2.6	No data
Peripheral orogenic belts (Superior)			**1.9–1.65**, 1.3–1.0	No data
Penokean (Southern) province	**2.5–2.2** (3.5)		1.9–1.8	140–170
Yavapai (Central) province	**1.8–1.5**			140–170
Greenland and Lewisian	**3.82–3.7**	2.9–2.5		No data
Grenville province	**1.4–1.0**			140–200
Cathaysian craton				
Yangtze craton	ePt, extensively reworked in Mz–Cz	1.85	1.05, 0.85–0.8	115–200
Orogenic belts at cratonic margins	**2.5–2.2, 1.86**			No data
Sino–Korean craton (Ordos, Ji-Lu nuclei)	**2.9–2.7** (3.57), extensively reworked in Mz–Cz	2.6–2.5, 2.2–1.9	1.8–1.7, 1.5–1.4	115–200
Tarim craton	**Ar–mPt**	1.9, 1.0	1.5–1.4, 1.0, 0.85–0.6	No data
Median massifs (e.g., Junggar, Songliao)	**0.8–0.6**			140–180
African craton				
Kaapvaal and Zimbabwe cratons	**3.5–3.2** (3.64)	3.2–3.0, 2.7–2.6	2.7–2.6	180–200
Peripheral orogenic belts, South Africa (e.g., Kheis, Magondi)	**2.0–1.8**			180–200
Mid–Proterozoic mobile belts, South and Central Africa (e.g., Namaqua–Natal, Irumides, Kibarian)	**1.3–1.0** (2.0)			120–140
Tanzanian craton	**3.0–2.6**		2.1–1.9	180–250
Central Africa (Angolian and Kasai cratons)	**3.5–3.4** and 3.0–2.6	2.7–2.55	2.1–1.75, 1.3, Pz–Mz	No data
Central Africa (Congo craton)	**Archean**, extensively reworked in Phanerozoic		1.0	No data
West African craton (Archean shields)	**3.0–2.9** (3.5)	2.7–2.55	2.0, 0.8–0.6	240–350
West African craton (Taoudeni Basin and Man shield)	Ar–ePt, extensively reworked at **2.2–1.9 Ga**		1.0	240–350
Benin–Nigeria Shield	(3.5–3.0)		2.75, 0.6	150–200
Trans-Saharan Belt and Tuareg Shield	? (3.5), extensively reworked at ~0.6 Ga	3.0, 2.1–1.95	1.1, 0.6	No data
Pan-African (Central African and Mozambique) mobile belts	**1.1–0.6**		0.65–0.55	90–140
Arabian–Nubian Shield	**0.95–0.68**			120–180
Antarctica				
Antarctic craton	Archean ? (3.8–3.93)	Unknown		No data

*Basement age refers to the oldest known major crust-forming event (see references in Goodwin, 1996) and it is not the age of the oldest known rocks (shown in brackets).
In bold — ages used to constrain the continental thermal model TC1 (Figs. 2, 10–13).

present global thermal model. Data on lithospheric thickness constrained by statistical relations between geological ages and mantle geotherms are used next to calculate the growth rate of lithospheric mantle since the Archean. Its comparison with growth models for the crust (e.g., Nelson and DePaolo, 1985; Patchett and

Arndt, 1986; Abbott et al., 2000) and with the age distribution of juvenile crust (Condie, 1998, 2001) permits speculations on the dynamic and tectonic evolution of the continents since the Archean.

2. Age of the continental lithosphere

The constraints of the present study depend critically on information on crustal ages. Data on the ages of the continental crust (based on Goodwin, 1996; Fitzgerald, 2002; Condie, 2005 and verified by regional geological and tectonic data) formed the basis of this study (Table 1). Seismic models have not been used to delimit tectonic terranes as exploited in some geophysical studies, because seismic anomalies in the mantle may reflect both thermal and compositional variations. A compilation of crustal ages averaged on a $1°\times1°$ grid is shown in Fig. 2. The following assumptions were made to constrain the age map.

(1) Because the goal of the study is to constrain a global model for the *present-day* thermal state of the continental lithosphere, the ages of the last major tectonic event (tectono-thermal ages) rather than the ages of the juvenile crust are used. For many Precambrian terranes, however, a distinction between geological age (i.e., the age of the major crust-forming event) and tectono-thermal age is speculative because major crust-forming episodes were probably caused by large-scale thermal and tectonic events (e.g., superplumes or plate tectonic processes resembling those of the present). Furthermore, some Archean–early Proterozoic terranes have undergone significant tectonic reworking in the Phanerozoic. These include, for example, the Wyoming, Sino–Korean, and Congo cratons, which were recognized as a separate category of "reworked Archean cratons". These cratons have been formed under unique temperature and compositional conditions during early evolution of the Earth (e.g., Abbott et al., 1994) and are expected to have preserved, in part, the distinctive structure and composition of the lithosphere, different from that of Phanerozoic terranes.

(2) In the further analysis it is assumed that the continental lithospheric mantle has the same age as the overlying crust, i.e., that they have been spatially and temporally linked since their formation, as indicated by Re–Os dating of mantle-derived cratonic xenoliths (Pearson, 1999). Recent high-resolution seismic transects have demonstrated that, at least in some Precambrian regions, this may not be true. For example, deep seismic reflection profiles across the margins of the Fennoscandian and the Slave cratons indicate that Archean lithosphere can underlie Proterozoic crust (e.g., BABEL Working Group, 1993; Cook et al., 1999); similar results have been obtained in a LITHOPROBE profile at the margin between the Superior and the Grenville provinces (Clowes et al., 1998). However, in all transects where an Archean block appears to underlie the Proterozoic lithosphere, its lateral extension underneath the younger crust does not exceed 100–200 km from the terrane boundary observed at the surface. Thus, because the lateral extent of the cratons commonly exceeds thousands of kilometers, the uncertainty associated with assigning lithospheric mantle the same ages as the overlying crust has little effect on this study.

(3) Basement ages in several regions with a thick sedimentary or ice cover are poorly known (e.g., Greenland, Antarctica, north-central and western Africa, central Australia, Yangtze craton, Rio Apa and Rio de la Plata cratons in South America), which precludes accurate model constraints (shown by question marks in Fig. 2). For these regions, the assigned ages are based on a limited number of isotope age data, chiefly from basement outcrops.

3. Statistical analysis of thermal model constrained by surface heat flow

The thermal model for stable continental regions constrained by surface heat flow data (Artemieva and Mooney, 2001) was analyzed for statistical relations between ages and mantle geotherms for five time intervals: the Archean, the early, middle and late Proterozoic, and the Paleozoic (Table 2). Furthermore, Archean terranes were subdivided into three groups which were analyzed separately: early Archean (older than 3.2–3.0 Ga), late Archean (3.0–2.5 Ga) and reworked Archean (with basement ages of 3.6–2.5 Ga).

I used data on lithospheric thermal thickness (defined as the intersection of the mantle geotherm with the 1300 °C mantle adiabat) to calculate typical lithospheric geotherms. Fig. 3 shows the thermal thickness of the continental lithosphere as a function of age. Despite a large scatter of thickness values (ca. 150 km for any of the considered age intervals)

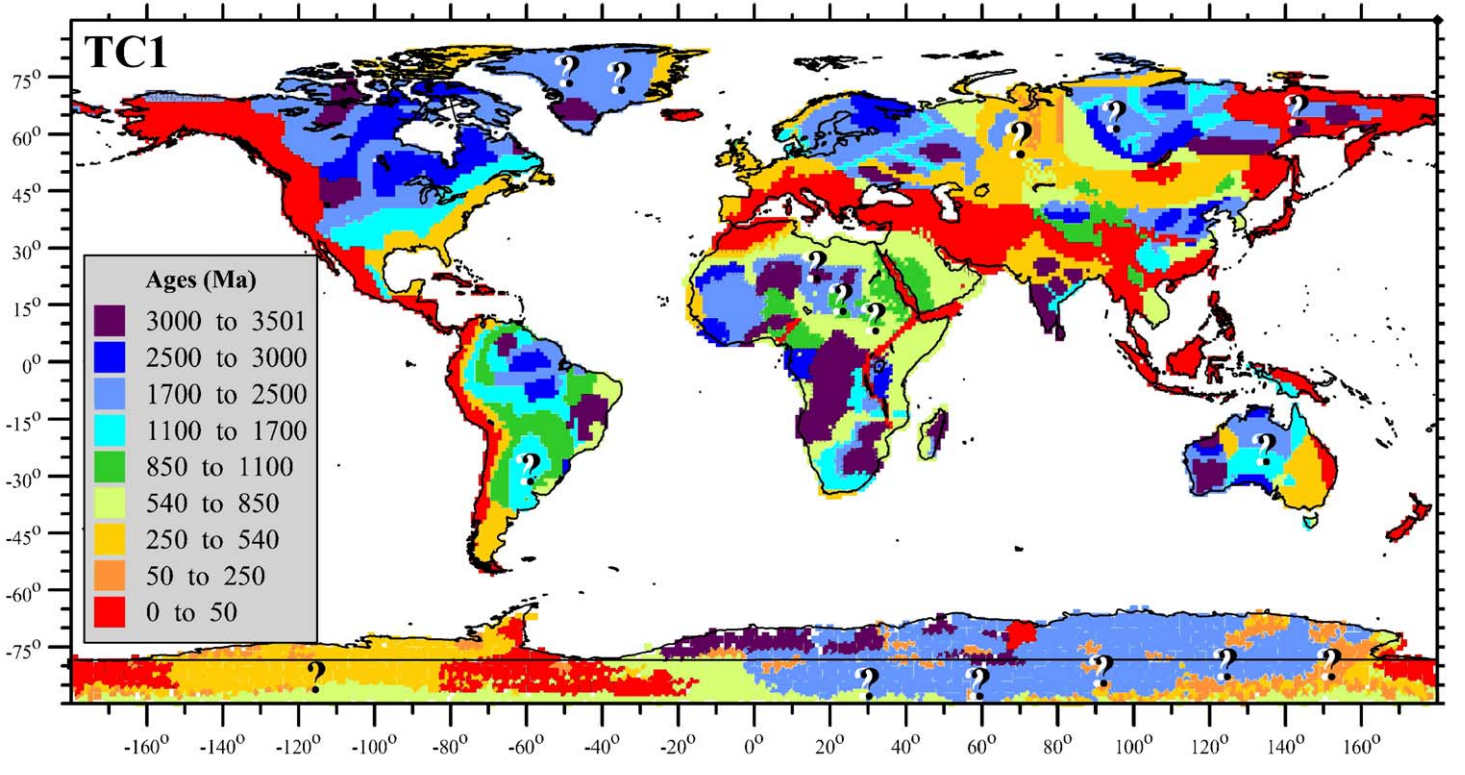

Fig. 2. Tectonic ages of the continents on a 1° × 1° grid (based on Goodwin, 1996; Fitzgerald, 2002; Condie, 2005, and numerous regional publications). The map shows the ages of the major crust-forming events (see Table 1), rather than ages of the juvenile crust, and forms the basis for the global thermal model for the continental lithosphere TC1.

Table 2
Statistics of thermal structure of the upper mantle for stable continental terranes (based on surface heat flow data)

	n	*T* at 50 km (°C)	*T* at 100 km (°C)	*T* at 150 km (°C)	Depth to 1300 °C (km)
Archean average	79	505±121	770±174	1010±201	219±73
Archean I (<3.0 Ga)	35	430±98	653±142	867±189	269±80
Archean II (>3.0 Ga)	33	527±67	809±76	1079±89	197±23
Archean III — reworked	11	691±77	1046±83	Above mantle adiabat	135±15
Early Proterozoic	56	592±98	871±126	1135±137	182±34
Middle Proterozoic	20	649±91	979±128	1261±111	153±25
Late Proterozoic	42	781±116	1154±146	Above mantle adiabat	121±24
Paleozoic	69	731±135	1102±181	Above mantle adiabat	130±30
Meso-Cenozoic	–	900 to 1200	Above mantle adiabat	Above mantle adiabat	60 to 90

associated with uncertainties of the thermal model (ca. 25% for the lithospheric thickness) and with diverse tectonic evolution for terranes of similar ages, there is a statistically significant correlation between the thermal state of the continental lithosphere and its age (Fig. 4a). Moreover, if all Archean terranes are considered as one group, the correlation is surprisingly high ($r=0.94$) with the average lithospheric

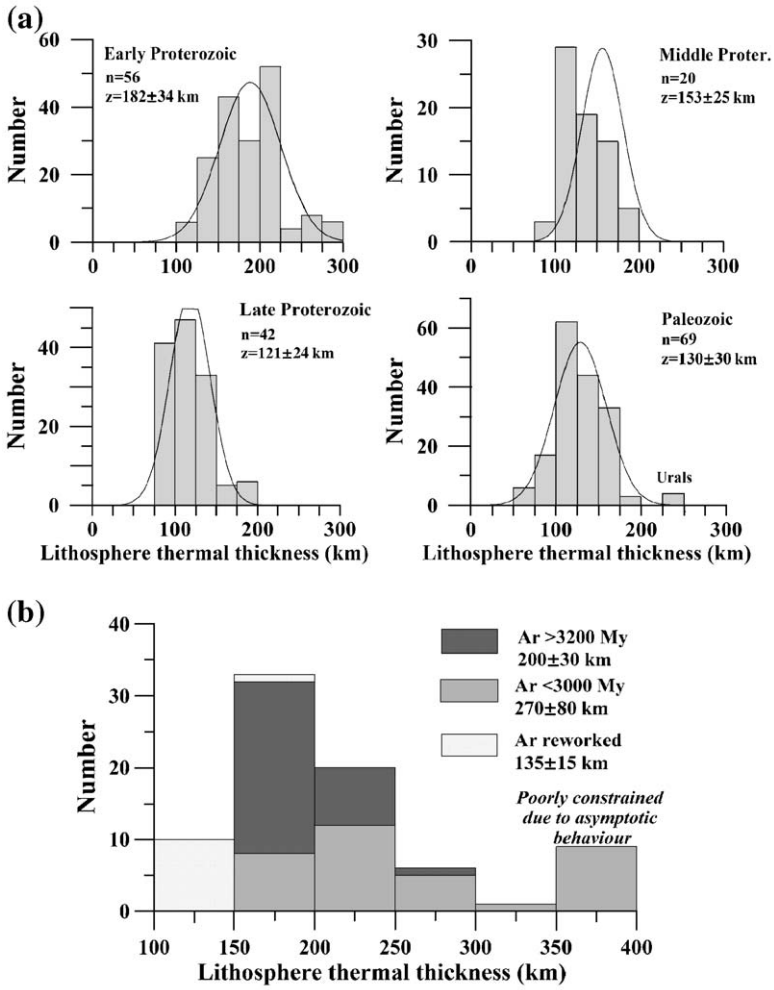

Fig. 3. Statistics of lithosphere thermal thickness based on heat flow data estimates (point data); (a) Proterozoic–Paleozoic terranes; (b) Archean terranes.

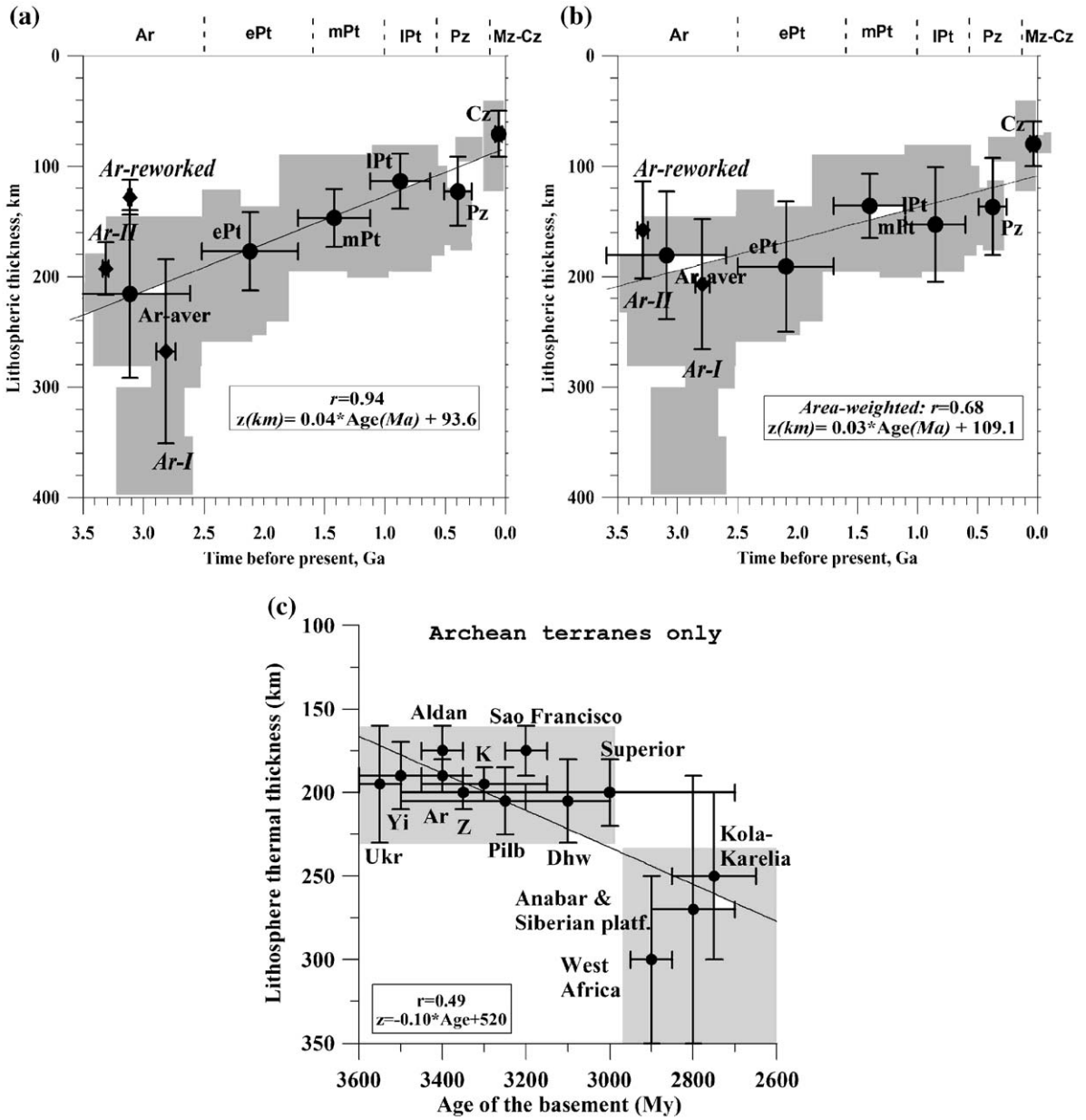

Fig. 4. Correlation between lithospheric thermal thickness and geological age of terranes. The bars indicate the scatter in the values, but not their uncertainties. (a) Global correlations for continents based on individual heat flow measurements; gray area shows the general trend of lithospheric thickness variations with age (Artemieva and Mooney, 2001); (b) Global correlations for continents, area-weighted on a 1°×1° grid for terranes of different ages; (c) correlations for Archean terranes; abbreviations: Ar=Aravalli, Dhw=Dharwar, K=Kaapvaal, Pilb=Pilbara, Yi=Yilgarn, Z=Zimbabwe cratons, Ukr=Ukrainian shield. Data for the Slave craton is not shown because only one heat flow measurement exists. Archean cratons are subdivided into three groups (Fig. 2 and Table 2): Ar-I includes cratons formed at 3.0–2.5 Ga, Ar-II includes mostly cratons of Gondwana-continents with basement ages>3.0 Ga, Ar-III includes cratons reworked by Phanerozoic tectono-magmatic events (e.g., Sino–Korean, Wyoming, Tanzanian and Congo cratons).

thickness z_{1300} (in km) showing a linear dependence on age t (in Ma):

$$z_{1300} = 0.04*t + 93.6, \quad (1)$$

while temperature gradient in the lithospheric mantle can be approximated as:

$$\frac{dT}{dz} = 537*(z_{1300})^{-0.88}. \quad (2)$$

It should be noted that these statistical relationships are not valid for some of the tectonic settings (e.g., for modern zones of continent–continent or continent–ocean collision or for Proterozoic terrains underlain by a dipping wedge of the Archean mantle). Furthermore, this statistics is significantly biased by the uneven distribution of heat flow measurements over terranes of different ages, which formed the basis for calculation of lithospheric geotherms (Artemieva and Mooney, 2001). Each value used in the statistical analysis corresponds to an area of $1° \times 1°$ to $5° \times 5°$ in size, where individual heat flow measurements in closely spaced boreholes were averaged for lithospheric blocks with similar crustal structure, ages, and tectonic setting. The correlation coefficient drops to $r = 0.68$ if the average values (Table 2) are area-weighted for terranes of different ages in order to remove the effect of uneven sampling by heat flow measurements (Fig. 4b).

As discussed in previous works (Artemieva and Mooney, 2001, 2002), Archean cratons appear to have two typical lithospheric thicknesses, 200–220 and 300–350 km, where cratons with shallower roots are located mostly on the Gondwana continents, while cratons with thicker roots are located mostly in the northern hemisphere (Table 1). The present analysis of the age relationship of the thermal state of the mantle (Fig. 4c) reveals that thick (>250 km) lithosphere is restricted solely to young Archean terranes (3.0–2.6 Ga), while in old Archean terranes (3.6–3.0 Ga) lithospheric roots do not extend deeper than 200–220 km.

Typical continental geotherms (Fig. 5) are constrained by heat flow data for stable continents and by xenolith data for active regions (Fig. 6f). They are in a general agreement with mantle temperatures calculated from joint interpretation of gravity and tomography models (Deschamps et al., 2002): the temperature difference between cratons, platforms, and tectonically active regions compared to the average mantle is, correspondingly, -310 ± 200, -160 ± 260, and $+30 \pm 130$ °C at 100 km depth and ca. -90 ± 70, -80 ± 100, and -30 ± 70 °C at 200 km depth (for average mantle temperatures of 1100 °C at 100 km depth and 1300 °C at 200 km depth).

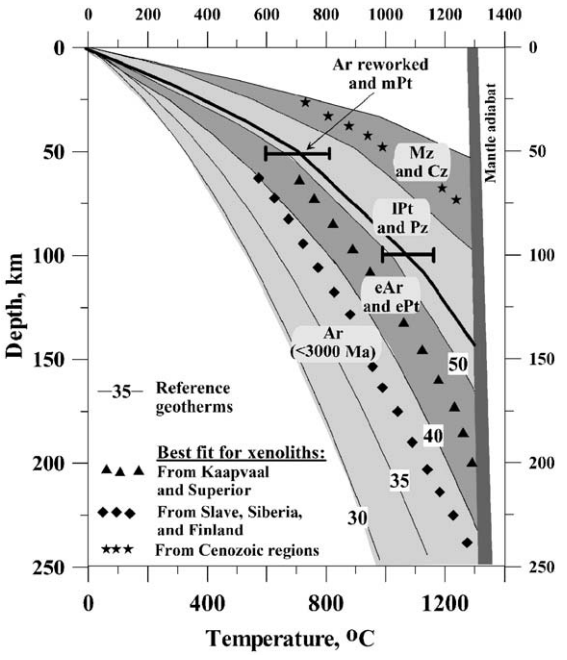

Fig. 5. Typical continental geotherms constrained by heat flow data for stable regions and by xenolith data for active regions. Five groups of typical geotherms include (from the coldest to the warmest): (a) Archean terranes younger than 3.0 Ga; (b) older Archean cratons (which include mostly cratons of Gondwana-continents) and early Proterozoic terranes; (c) reworked Archean cratons that have mantle temperatures similar to middle Proterozoic terranes (shown by line with bars); (d) Paleozoic and late Proterozoic regions; (e) Meso-Cenozoic regions. Thin lines—conductive geotherms of Pollack and Chapman (1977), values are surface heat flow in mW/m^2.

4. Xenolith constraints on mantle geotherms and lithospheric thickness

Xenolith P–T arrays (xenolith geotherms) provide valuable independent control on the thermal state of the lithosphere. A large set of geothermobarometers (e.g., reviewed by Smith, 1999) has been proposed to determine temperature and equilibrium pressure (i.e., the depth of origin) of individual mineral grains in mantle-derived xenoliths at the time when they were entrained into the host volcanic rock. These P–T arrays are strongly dependent on the geothermobarometers employed. For example, the difference in pressure between the BKN (Brey et al., 1990) and NT (Nimis and Taylor, 2000) geobarometers can be as large as ±10 kbar (Grutter and Moore, 2003); the scatter of equilibration temperatures determined with FB (Finnerty and Boyd, 1987) and NT thermometers reaches 200 °C but decreases with temperature increase (Preston and Sweeney, 2003). Furthermore, xenolith geotherms based on *opx–grt* geothermobarometers (e.g., the BKN and FB methods) have the same temperature gradient as the conductive geotherms of Pollack and Chapman (1977), while P–T arrays constrained by *cpx–grt* NT barometers have smaller gradients and thus intersect the mantle adiabat at a shallower depth (Grutter and Moore, 2003). For these reasons, comparison of xenolith P–T arrays constrained by different geothermobarometers can be misleading.

For simplicity and following a widely accepted practice in petrological community, I further compare

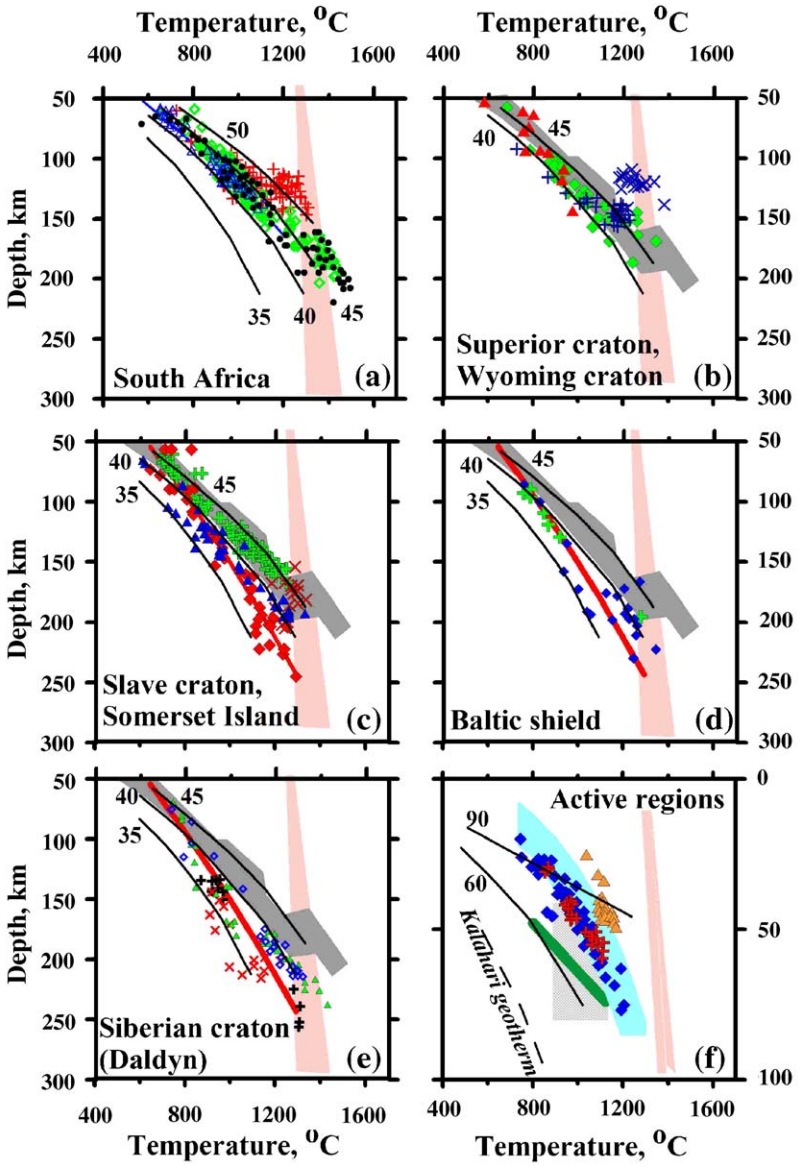

Fig. 6. Xenolith geotherms for continents clearly indicate two typical cratonic geotherms: ~45 mWm^2 (a, b) and ~37 mWm^2 (c–e). Because xenolith *P–T* arrays constrained by different geothermobarometers are significantly different, the data are shown mostly for the BKN method (Brey et al., 1990); data obtained with other calibrations is keyed as NT (Nimis and Taylor, 2000), MC (MacGregor, 1974), FB (Finnerty and Boyd, 1987) and ONW (O'Neill and Wood, 1979). Thin lines—conductive geotherms of Pollack and Chapman (1977), values are surface heat flow in mW/m^2. Pink shading—mantle adiabat. (a) South Africa: blue triangles—Kimberly (Kaapvaal), green rhombs—Lesotho, red crosses—Gideon, Namibia (all three BKN-NT data from Grutter and Moore, 2003); black circles—xenolith data from several locations in Kaapvaal (compilation of Rudnick and Nyblade, 1999); these data are shown in plots (b–e) by gray shading; (b) Superior craton (Kirkland Lake)—green rhombs (data from Pearson et al., 1998); Wyoming craton—blue pluses (NT–NT data from Pizzolato and Schultze, 2003) and blue crosses (BKN data from Hearn, 2003); red triangles—SW Arkansas (BKN data from Dunn et al., 2003); (c) Slave craton: red rhombs—low-*T* peridotites (red line shows the best-fit) (BKN data from Kopylova et al., 1999; Kopylova and McCammon, 2003), red crosses—high-*T* peridotites (BKN data from Kopylova and McCammon, 2003); blue triangles—Lac de Gras area (BKN data from Menzies et al., 2003); green pluses—Somerset Island (MC-NT data from Grutter and Moore, 2003); (d) Fennoscandia: blue rhombs—central Finland (BKN data from Kukkonen and Peltonen, 1999; Lehtonen et al., 2003); green crosses—Arkhangelsk, pipe Grib (BK-MC data from Malkovets et al., 2003); red line—best fit for the Slave craton; (e) Siberian craton (Daldyn terrane): blue rhombs and green triangles (correspondingly, FB and ONW data from Griffin et al., 1996); black pluses—Zarnitsa pipe, red crosses—Irelyakhskaya pipe (both NT–NT data from Aschepkov et al., 2003); (f) active regions: orange triangles—SE China (data from Xu et al., 1996); blue diamonds—SE Australia (data from O'Reilly and Griffin, 1985); red crosses—Tariat region, Mongolia (data from Ionov et al., 1998); blue shading—Baikal region: Sayans, Vitim, and Udokan (data from Litasov et al., 2003); green line—Rhenish massif (after Le Bas, 1987); hatched area—Massif Central (after Coisy and Nicolas, 1978; Masse, 1983); for a comparison a typical Kalahari geotherm is shown by dashed line (Rudnick and Nyblade, 1999). Note different depth scale of the plot.

Table 3
Thermal structure of cratonic mantle from xenolith data

Location	Age of emplacement	Lithospheric thickness (km) from xenolith data	Reference geotherm (mW/m^2)	Reference
Africa				
Kaapvaal	90 Ma, 120 Ma, 1180 Ma	200–250	40*	RN99;
		180–200	40*	G93; R96;
		~180	39*	BG86
Lesotho		170–190	40*	R96; BG86;
Tanzania		~150	–	ORG96; LR99
Namibia		~200 (MBL)	–	P94
Mobile belts of S. Africa		~140	–	BG86
Siberia				
Daldyn–Alakit (Udachnaya)	Permian–Devonian, 345–360 Ma	~240	~35*	G99
		–	40*	B84
		–	34*	R96
Malo–Botuobinsk (Mir)	Permian–Devonian, 345–360 Ma	~220	~35*	B76; G93; G96; P91
		200–250?	40*	RN99; G99
Muna	Permian–Devonian, 345–360 Ma	–	38*	G99
North America				
Slave	170 Ma	200–250	40**	RN99
		200–220	35–38*	OR01
		160–190 (N)	37–40**	K99
		200 (Central)	–	P99
		>230 (South)	–	K01
Slave (Lac de Gras)	47–53 Ma	–	37–40*	Me03
Superior (Wawa)	140 Ma	200–250	37–40*	Kj99
		–	40**	RN99
Superior (Kirkland Lake)	140 Ma	–	42*	P98
Trans-Hudson Orogen		–	~40*	Kj99
Saskatchewan	Cretaceous	–	42*	Kj99
Wyoming craton	48–52 Ma	~140?	–	E88
		–	40*	R96
Somerset Isl. (Canadian Shield)	99 Ma	–	44*	SF99
Asia				
Sino–Korean craton	Paleozoic	180	40*	ORG96
		140	–	G98, X00
Australia				
E.Australia	Permian, Mesozoic	~80–100	~90*	ORG85
South America				
Brasil (Sao Francisco craton)	80–90 Ma	–	34–40* (>89 Ma)	R03
		–	39–50* (80–85 Ma)	R03
Europe				
Central Finland	Early Proterozoic	220	36*	PD99,
		200–240 (MBL>240)	–	KP99
Arkhangelsk region	Devonian	>200	–	PD99
		–	37–38*	M03
Kola Province	Devonian	~150	–	PD99
SvecoFennian	Late Paleozoic	~150	–	PD99

Table 3 (*continued*)

Location	Age of emplacement	Lithospheric thickness (km) from xenolith data	Reference geotherm (mW/m^2)	Reference
Scania, S.Sweden	Tertiary	<100	–	PD99
SW.Norway	Tertiary	<100	–	PD99

*Reference geotherms of Pollack and Chapman (1977).

**Geotherms calculated in the original publications (see references).

References: B76=Boyd et al., 1976; B84=Boyd, 1984; BG86=Boyd and Gurney, 1986; E88=Eggler et al., 1988; G93=Griffin et al., 1993; G96=Griffin et al., 1996; G98=Griffin et al., 1998b; G99=Griffin et al., 1999; Kj99=Kjarsgaard, 1999; K99=Kopylova et al., 1999; K01=Kopylova and Caro, 2001; KP99=Kukkonen and Peltonen, 1999; LR99=Lee and Rudnick, 1999; M03=Malkovets et al., 2003; Me03=Menzies et al., 2003; ORG95=O'Reilly and Griffin, 1985; ORG96=O'Reilly and Griffin, 1996; OR01=O'Reilly et al., 2001; PD99=Poudjom Djomani et al., 1999; P91=Pokhilenko et al., 1991; P94=Pearson et al., 1994; P99=Pearson et al., 1999; RN99=Rudnick and Nyblade (1999); R03=Read et al., 2003; R96=Ryan et al., 1996; SF99=Schmidberger and Francis, 1999; X00=Xu et al., 2000.

xenolith geotherms with the family of reference conductive geotherms of Pollack and Chapman (1977), which were constrained under an assumption (based on the data set of 9 points only) that 60% of the surface heat flow comes from the mantle. Petrological and thermal data show that average crustal heat production depends on the crustal age, being the lowest for the Archean crust and increasing to Phanerozoic (e.g., Rudnick et al., 1998). Thus, for the Archean crust the assumption of Pollack and Chapman (1977) is the weakest and extrapolation of reference geotherms to the surface heat flow should be interpreted with caution. Nevertheless, the set of reference geotherms provides a simple frame for a comparison of mantle thermal regime constrained by different methods.

Fig. 6 shows a compilation of xenolith *P–T* arrays for Precambrian cratons and Phanerozoic regions; a pressure-to-depth conversion was based on crustal and mantle densities of 2.7 and 3.3 g/cc, correspondingly. Earlier, Rudnick and Nyblade (1999) compiled xenolith *P–T* arrays for Kaapvaal, Siberia, Slave and Superior cratons and concluded that all of them fall onto the same mantle geotherm. The present analysis with a preferred choice of *P–T* arrays constrained (where available) by the BKN method and with a distinction of xenolith *P–T* data from different kimberlite pipes within a craton does not support this conclusion.

Xenolith geotherms from Kaapvaal, Namibia, Superior province, Wyoming craton, and Somerset Island (Northern Canada) follow the 40–45 mW/m^2 conductive geotherm (except for a high-temperature part which can be attributed to plume-related effects, Sleep, 2003), whereas *P–T* arrays from the Slave craton, Fennoscandia (central Finland and Arkhangelsk region), and the Siberian platform indicate a colder geotherm, 35–38 mW/m^2 (Table 3). This difference in xenolith geotherms implies a significant difference in lithospheric thickness. Ignoring the existence of a rheologically active boundary layer with perturbed geotherm between the conductive thermal boundary layer and the convecting mantle, a 42 mW/m^2 geotherm intersects the mantle adiabat at ca. 220 km depth, while a 37 mW/m^2 geotherm—at ca. 300 km depth. Xenolith geotherms from the Superior craton, from some kimberlite pipes of the Slave craton, and from the Trans-Hudson orogen (with the buried Archean Sask craton) indicate temperatures of ca. 900±50 °C at 150 km depth (Griffin et al., 2003). This places these parts of the Canadian shield into the group of the Archean–Paleoproterozoic cratons with thick (>250 km) lithospheric roots (Figs. 4c, 5). Thus, xenolith data support

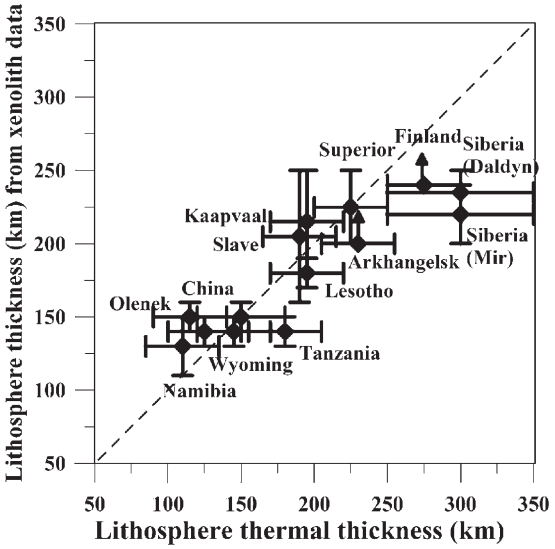

Fig. 7. Correlation between lithospheric thickness constrained by heat flow and xenolith geotherms for stable continental terranes. Note that the bars show the range of thickness estimates for different cratonic blocks, but not an uncertainty. Because the deepest known kimberlite magmas originated at ca. 250 km depth, xenolith and thermal constrains on lithospheric thickness diverge at greater depth. However, xenoliths from Finland derived from 240 km depth do not show shearing and suggest lithospheric thickness greater than 240 km (shown by an arrow).

the conclusion of the existence of cratonic terranes with two characteristic thicknesses, 200–220 km and ca. 300 km (Artemieva and Mooney, 2001), further supported by convection modeling (Doin et al., 1997).

The thermal and xenolith geotherms agree well for Precambrian terranes with mantle geotherms above the 40 mW/m^2 reference geotherm (Fig. 7). A significant discrepancy observed for terranes with colder geotherms (Siberia and Baltic shield) can be attributed to the fact that the deepest known mantle xenoliths came from ca. 200–240 km depth and did not sample deeper layers. Kimberlite magmas from deeper mantle either do not reach the surface due to their low-percentage melting or are not generated deeper than 240–250 km depth. However, even the deepest xenoliths from the Baltic shield (ca. 240 km depth) do not show shearing associated with flow in the rheologically active boundary layer beneath the base of the conductive thermal boundary layer (Kukkonen and Peltonen, 1999). This implies thicknesses of lithospheric roots greater than 240 km (shown by arrows in Fig. 7).

Xenolith *P–T* arrays from different regions of Cenozoic extension, rifting, and volcanism are surprisingly similar and indicate high mantle geotherms, which intersect the mantle adiabat at a depth of 60–100 km (Fig. 6f). These data were used to constrain the thermal regime of the lithosphere of tectonically active regions (Fig. 5).

5. Constraints on continental geotherms from electrical conductivity

Strong, exponential dependence of electrical conductivity on temperature provides a possibility to constrain mantle geotherms from conductivity–depth profiles (e.g., Shankland and Duba, 1990). However, the true resistivity of the lithospheric mantle is poorly resolved

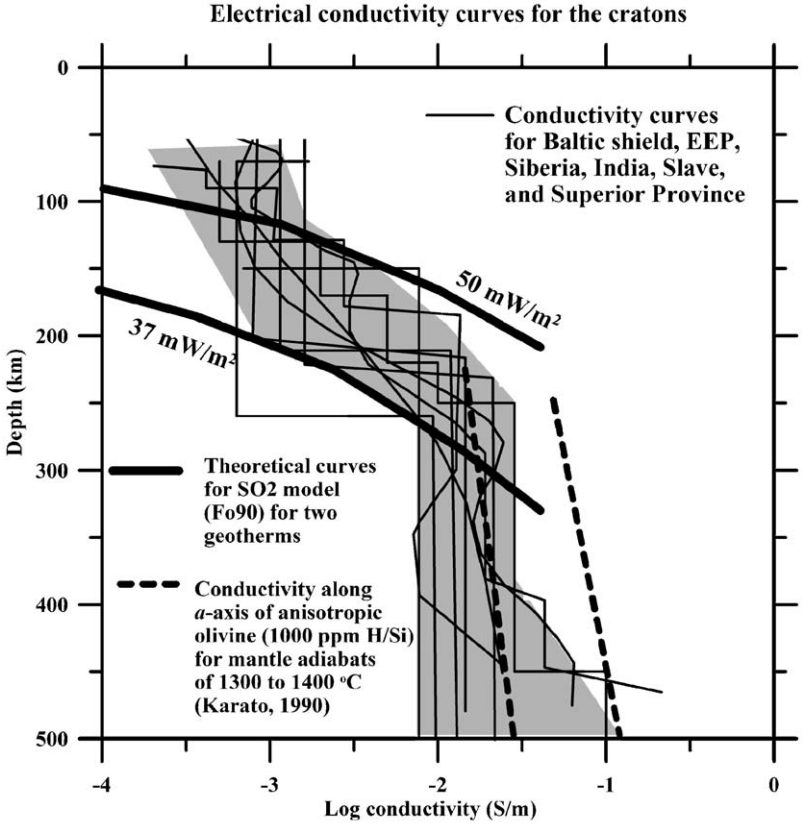

Fig. 8. Electrical conductivity profiles for different cratonic regions of the world: Baltic shield (Korja, 1993; Korja et al., 2002), East European craton (Vanyan et al., 1977), Ukrainian Shield (Zhdanov et al., 1986), Siberia (Safonov et al., 1976; Vanyan and Cox, 1983; Singh et al., 1995), India (Singh et al., 1995), Slave craton (Wu et al., 2002; Jones et al., 2003), and Superior Province (Schultz et al., 1993; Kurtz et al., 1993; Mareschal et al., 1995; Neal et al., 2000). Also shown are synthetic conductivity curves calculated for conductive continental geotherms of 37 and 50 mW/m^2 for the standard olivine model SO2 (Constable et al., 1992) with 90% of forsterite (thick solid lines) and conductivity along *a*-axis of anisotropic wet olivine (1000 ppm H/Si) for mantle adiabats of 1300 to 1400 °C (Karato, 1990) (thick dashed lines). It is important to note that all cratonic conductivity curves fall between theoretical conductivity estimates for 37 and 50 mW/m^2 conductive geotherms, in agreement with thermal (Fig. 5) and xenolith (Fig. 6) constraints.

and the uncertainty is often larger than an order of magnitude (e.g., Jones, 1999), while the vertical resolution of the MT surveys typically is ca. 5–10% of sampled depth (e.g., Hjelt and Korja, 1993). I have compiled conductivity–depth profiles constrained by long-period MT and GDS studies for different cratons of the world (Fig. 8). Some earlier results were excluded from the compilation as unreliable; for example, there are still doubts if source field problems associated with high latitudes can cause misinterpretations of natural-source MT data in northern parts of the Baltic shield (Osipova et al., 1989).

There is a striking agreement between the general pattern of the upper mantle conductivity for all of the cratons (Fig. 8). Using experimental studies of electrical conductivity of olivine, which supposedly comprises about 50–60% of the upper mantle and thus essentially controls mantle conductivity, Constable et al. (1992) proposed a reference conductivity–temperature curve (the SO2 model) for dry subsolidus olivine. I used the SO2 model to calculate theoretical conductivity–depth profiles in the mantle for two reference conductive geotherms.

Fig. 8 clearly shows that, in the depth range between 100–150 and 220–280 km, measured electrical conductivity of cratonic lithosphere falls between theoretical conductivity curves for typical cratonic geotherms of 37 and 50 mW/m^2, and thus confirms cratonic geotherms constrained by thermal and xenolith data. The deflection of regional conductivity models from the synthetic conductivity curve above 100–150 km depth can be attributed to the presence of highly conductive phases. For typical cratonic geotherms the graphite–diamond transition occurs at a depth of 120–170 km (Kennedy and Kennedy, 1976); because diamonds are abundant in cratonic roots, it is reasonable to attribute an order of magnitude increase in conductivity of the uppermost mantle to the presence of graphite. Conducting graphite films were also used to explain electrical anisotropy in the upper 100 km of the mantle beneath the Superior craton (Mareschal et al., 1995).

For a typical cratonic conductivity model, the bottom of the electrical lithosphere is expected to be at a depth of ca. 220–260 km. At this depth, a transition from

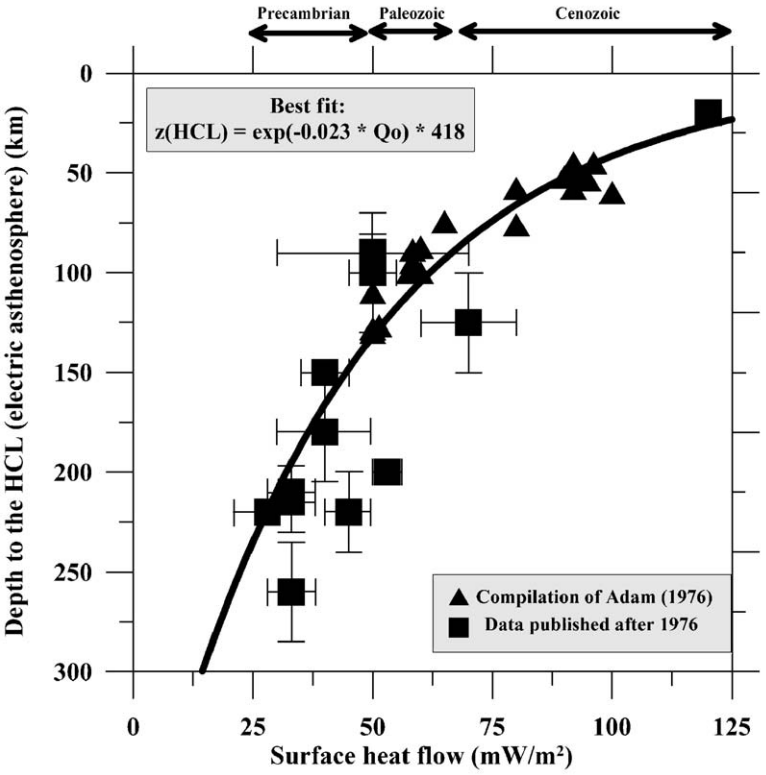

Fig. 9. Correlation between surface heat flow and depth to the high-conductive layer in the mantle (electric asthenosphere). Depth to HCL is based on interpretations of Adam (1976), Adam and Wesztergom (2001), Bahr (1985), Berdichevsky et al. (1980), ERCEUGT-Group (1992), Jones et al. (2003), Korja (1993), Kurtz et al. (1993), Mareschal et al. (1995), Moroz and Pospeev (1985), Safonov et al. (1976), Schultz et al. (1993), Simpson (2002), Singh et al. (1995), Vanyan and Cox (1983), Zhdanov et al. (1986). The curve can be used as a proxy to the depth of the HCL for regions with a known heat flow.

conductive to adiabatic geotherm leads to a step-like change of conductivity curves due to a weak depth dependence of conductivity in the high-conductivity layer, HCL (interpreted as electrically conductive asthenosphere).

Assuming surface heat flow is representative of mantle temperatures (which is not true in regions with a transient thermal regime, anomalous crustal radioactivity, or intense groundwater circulation that affects borehole heat flow measurements), Adam (1976) proposed that the depth to the HCL (i.e., presumably the depth where partial melting of mantle material starts) correlates with the surface heat flow on the continents. An update of this compilation for electrical conductivity models published over the past three decades further suggests that, under certain assumptions, surface heat flow can be used as a rough proxy for the depth of the HCL (Fig. 9). In particular, a correlation between the depth to the HCL (z_{HCL}, in km) and surface heat flow (Q_o, in mW/m^2) can be approximated as:

$$z_{HCL} = 418*\exp(-0.023*Q_o). \quad (3)$$

Because surface heat flow is, in general, age-dependent (Pollack et al., 1993), this implies that the depth to the HCL should correlate with crustal age as well. Nevertheless, due to the large uncertainty in interpretations of electromagnetic data, the correlation between surface heat flow and the depth to the HCL should be considered with extreme caution, and especially for cratonic regions with $Q_o < 50$ mW/m^2, where the correlation between the two parameters is very weak (Fig. 9).

6. Global thermal model TC1 of continental lithosphere

6.1. Model constraints and major assumptions

Lithospheric geotherms based on statistical analysis of the thermal model for terranes of different ages (Figs. 3–5) and supported by xenolith and electromagnetic data (Figs. 6, 8) were used to constrain a global thermal model of the continental lithosphere on a 1° × 1° grid (Figs. 10–13).

(1) For stable continental regions where reliable heat flow measurements exist (ca. 40% of the continents, Fig. 1) mantle temperatures reported in the previous work (Artemieva and Mooney, 2001) were used. For regions with no or unreliable heat flow measurements the statistical values were assigned depending on the age and tectonic setting (Tables 1, 2 and Fig. 2).

(2) For several tectonic settings the statistical relationships were not used. Lithospheric geotherms in tectonically active continental regions (regions of Cenozoic extension, rifting, and volcanism) were assumed to reach 1300 °C at a depth of 60–100 km as indicated by xenolith geotherms (Fig. 6), while the lithospheric thickness in modern zones of continent–continent or continent–ocean collision (Andes, Hellenic arc, Alps) was fixed at 220 km. This value is supported by regional seismic tomography studies in continental collisional orogens where the presence of subducted lithospheric slab in the upper mantle is interpreted down to depths of 200–250 km (e.g., Spakman, 1990). Tibet was assumed to be underlain by the Archean lithosphere of the Indian craton as suggested by recent seismic studies (e.g., Tilmann et al., 2003).

(3) Archean cratons were subdivided into three groups: I—late Archean (3.0–2.5 Ga), II—early Archean (3.6–3.0 Ga), III—reworked Archean. Xenolith P–T arrays (Fig. 6) and electrical conductivity curves for cratonic mantle (Fig. 8) support a diversity in thermal structure of the Archean lithosphere: typical geotherms range from 35–38 mW/m^2 (mostly in late Archean cratons) to 40–45 mW/m^2 (mostly in early Archean cratons). In accord with the results of thermal modeling, xenolith geotherms indicate colder conductive geotherms for the late Archean Baltic shield, Siberian and Slave cratons (group I). In agreement with these data and Fig. 4c, it was assumed that beneath the early Archean terranes of Central and Southern Africa, South America, Labrador, and Greenland (group II, Fig. 2) the mantle adiabat is reached at 220 km depth, while beneath the south-central part of the Slave carton, the north-eastern part of the Superior craton (Ungawa block), Rae, and Hearne cratons in North America the lithospheric thermal thickness is 300 km.

A subdivision of Archean cratons into two age groups (I and II) is indirectly supported by the diversity of their crustal structure. Windley (1995) recognizes four different types of Archean crust: (a) the Kaapvaal craton which has undergone a stage of intraoceanic tectonics followed by a stage of intracontinental tectonics; (b) cratons formed at an active continental margin (Greenland, Labrador, NW Scotland); (c) cratons formed at a passive continental margin (India and NE China); and (d) cratons formed by a collision of island arcs (the Superior province and the Slave craton). Moreover, cratons of the

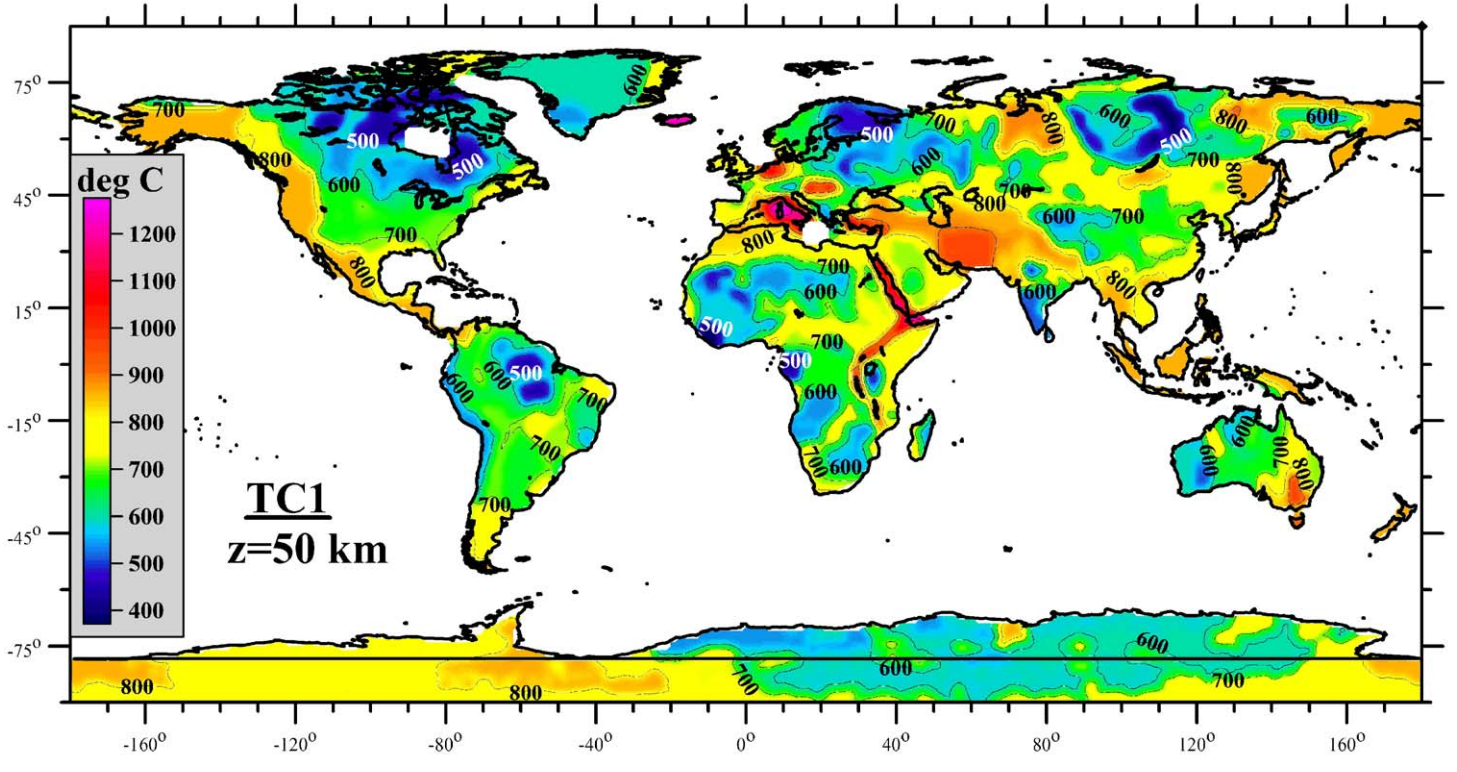

Fig. 10. Global thermal model for the continental lithosphere TC1 constrained on a 1°×1° grid: temperature at a 50 km depth interpolated with a low-pass filter.

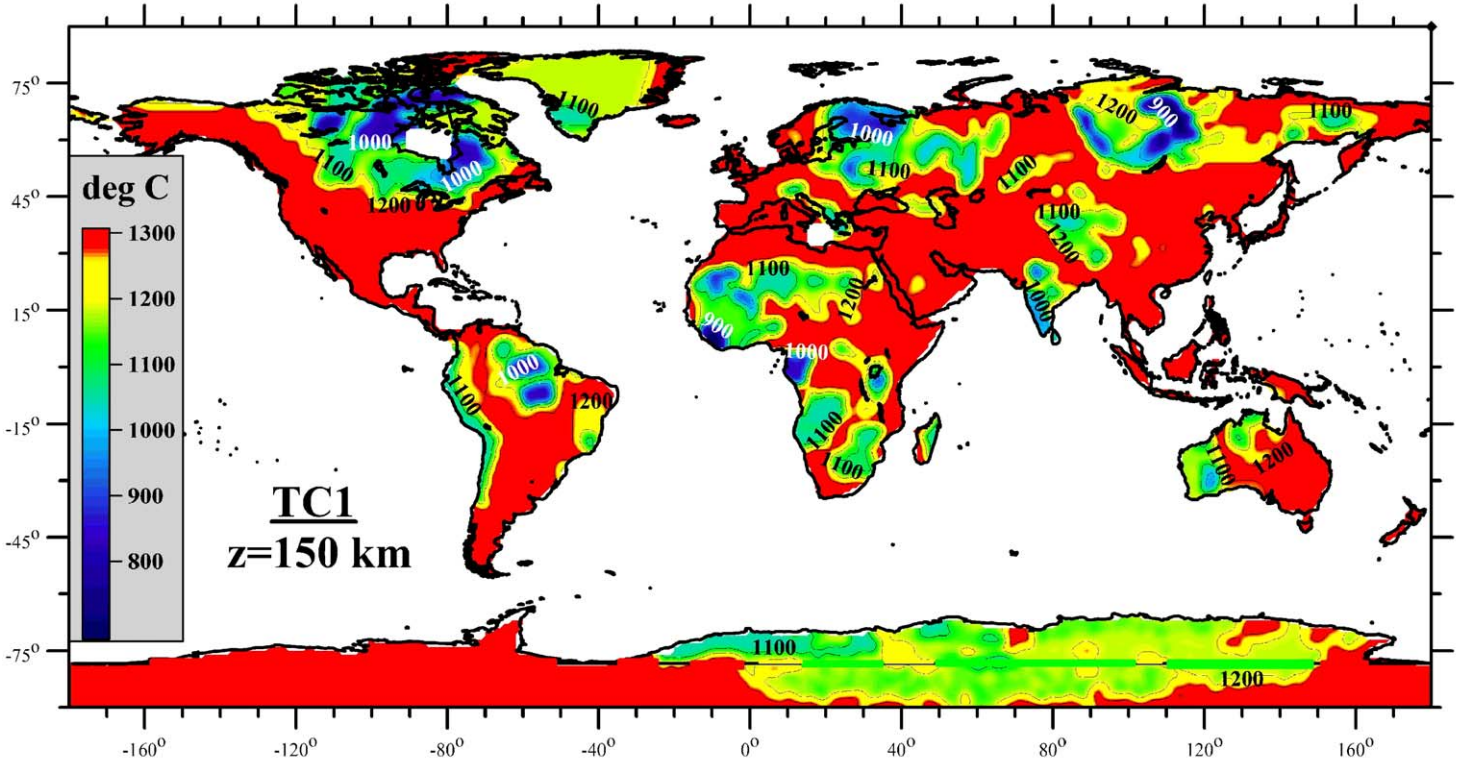

Fig. 11. Global thermal model for the continental lithosphere TC1 constrained on a 1° × 1° grid: temperature at a 150 km depth interpolated with a low-pass filter.

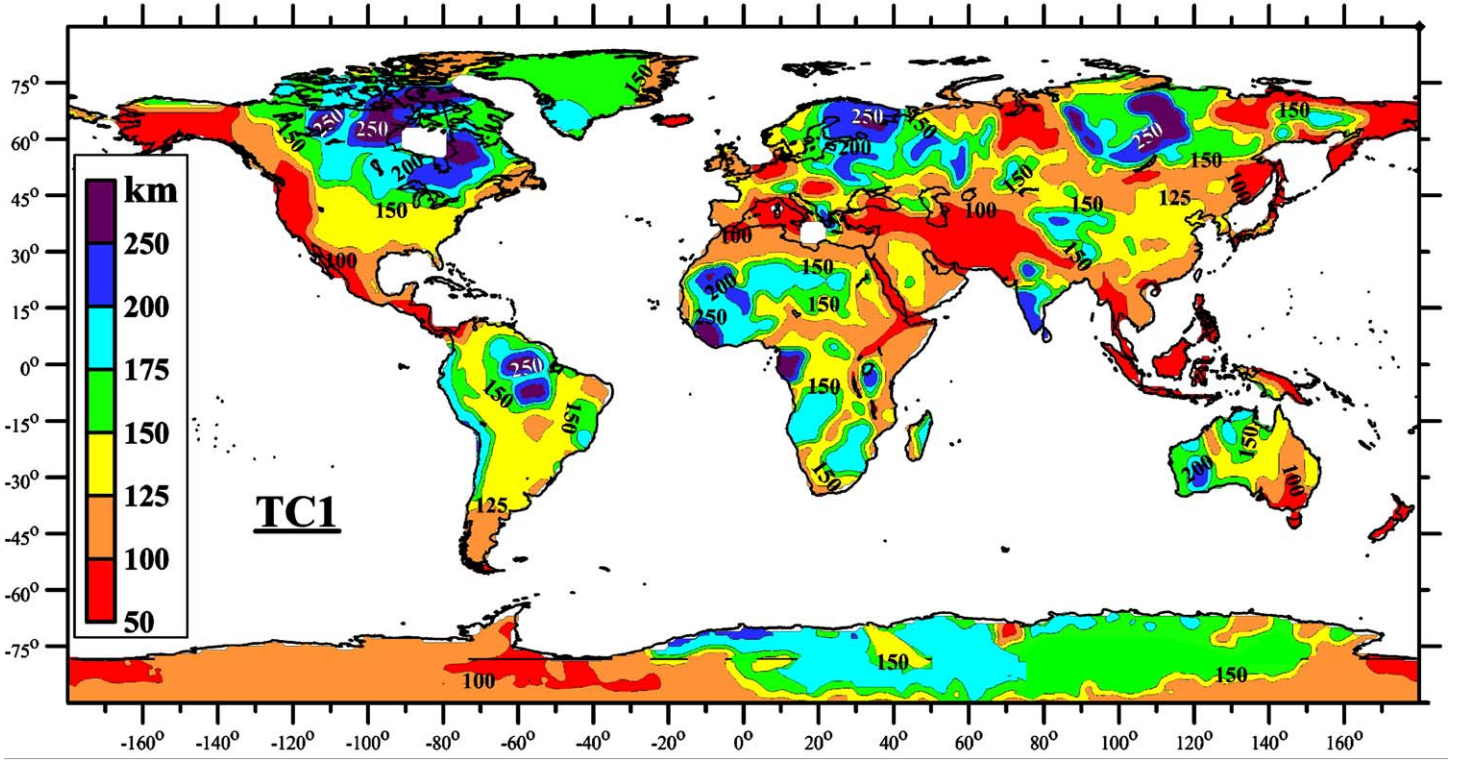

Fig. 12. Global thermal model for the continental lithosphere TC1 constrained on a 1° × 1° grid: lithospheric thermal thickness interpolated with a low-pass filter. The values are based on typical continental geotherms (Figs. 3–6) and tectonic age of the basement (Fig. 2).

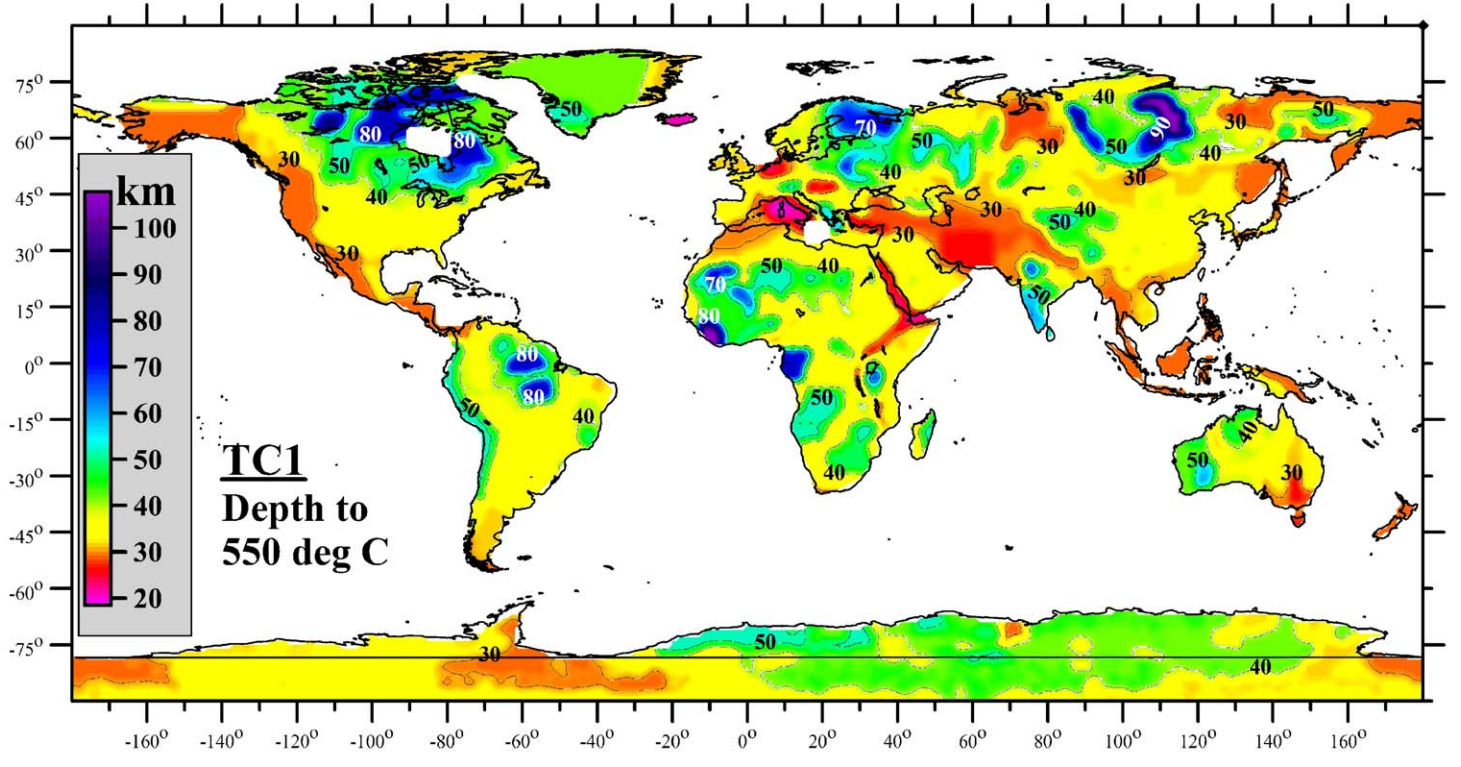

Fig. 13. Global thermal model for the continental lithosphere TC1 constrained on a 1° × 1° grid: depth to the 550 °C isotherm interpolated with a low-pass filter. This depth can be considered a proxy of the thickness of magnetic crust (Petersen and Bleil, 1982) and as a proxy for the depth to the brittle–ductile transition in mantle olivine (Kusznir and Karner, 1985).

first two types have a well-documented geological and tectonic history from late to early Archean; whereas no early-mid-Archean history is known for the two last types of Archean cratons.

6.2. The TC1 model: some examples

(1) The constraints for some of the continental regions with no heat flow data require a comment. I next discuss the Congo craton as an example, because it is one of the largest unexplored Archean cratons where no modern geological mapping or regional geophysical studies have been done. Recently Lucazeau et al. (2004) reported heat flow measurements for the passive margin of the lower Congo basin off-shore Angola; however, no heat flow measurements have been done so far within the internal parts of the craton. Its crustal structure is also unknown. The craton is covered by Palaeozoic to recent sediments that formed during the opening of the Atlantic and the separation of the Congo and Brazilian Archean shields. The thickness of sediments is unknown; the CRUST 2.0 model assumes it varies from 0.5 to ca. 7 km in the central part of the vast area of the Congo basin (Laske and Master, 1997). Large sedimentary thickness suggests that lithospheric mantle of the Archean Congo basin could have been significantly affected by Phanerozoic large-scale thermal perturbations in the mantle. Similar to the Sino–Korean craton, this could have resulted both in lithosphere erosion/delamination and its chemical modification by metasomatism. Thus, I assume that the lithospheric structure of the Congo craton is similar to other reworked Archean cratons (group III) and that its thermal thickness is ca. 120–150 km (Fig. 12).

These values, however, contradict regional surface wave tomography results which indicate high mantle seismic velocities down to a depth of 200–250 km (Ritsema and van Heijst, 2000). A large part of this discrepancy can, probably, be attributed to incomplete crustal correction of the seismic data because the crustal structure of the craton is unknown. Theoretical analysis of the crustal effect on the global phase velocity maps of Rayleigh waves at a period of 150s indicates that the crustal contribution can be as large as 50% of the total signal and with the sign opposite to the mantle contribution (Laske and Master, 1997). In case of large basins even small errors in data on the thickness of the sedimentary cover can produce significant errors in seismic models: for example, a 1 km underestimation of the sedimentary thickness produces a +1% erroneous increase in phase velocities, while a 3 km overestimation of sediments produces a velocity error of ca. +2.5% (Bassin et al., 2000). Thus, a +2% +3% velocity anomaly at 200 km depth beneath the Congo basin can result from a 3 km underestimate of the sedimentary thickness in the region where practically no geophysical data exist.

(2) Antarctica is another example of a huge continental region with almost no borehole heat flow measurements (Engelhardt, 2004) and very limited geophysical data on its lithospheric structure. Recently, several attempts have been done to estimate the thermal regime of the continent using seismic tomography (Shapiro and Ritzwoller, 2004a,b; Kuge and Fukao, 2005) and satellite magnetic data (Maule et al., 2005). The TC1 model, based on the sparse available age data for Antarctica and the statistical relationship (Eq. 1), shows mantle temperatures in the East Antarctic craton that are ca. 100–150 °C higher than estimated in a seismic tomography model (Kuge and Fukao, 2005). The discrepancy between these results can be attributed both to the poorly known geological and tectonic history of Antarctica and to its poorly known crustal structure.

Because the Curie temperature for magnetite is close to 550 °C (Petersen and Bleil, 1982), the depth to this isotherm can be interpreted as the maximal depth of crustal magnetization and can be considered as a proxy for the thickness of magnetic layer (Fig. 13). The TC1 model predicts the depth to the Curie isotherm to be 40–50 km in the Precambrian part of Antarctica and less than 30 km in its Phanerozoic part. These values are close to the thickness of the magnetic crust as calculated from satellite magnetic data: 40 to 60 km in the East Antarctic craton and <20 km in the West Antarctic rift system (Maule et al., 2005). Thus, magsat data support the TC1 model for Antarctica.

(3) The depth to the 550 °C isotherm (Fig. 13) can also be interpreted as the elastic thicknesses of the continental lithosphere, where this depth exceeds the crustal thickness. Lithospheric strength envelopes based on deformation models with a constant strain rate and constant mineralogy associate a peak in the strength of the continental lithosphere at the top of the mantle with the transition from a quartz to an olivine rheology (e.g., Kohlstedt et al., 1995). Laboratory data on rock deformation and thermal models of intra-plate basin formation predict that flexural rigidity of old (>200 Ma) continental lithosphere is dominated by an olivine rheology of the mantle with a critical isotherm of ~550 °C (Kusznir and Karner, 1985). However, for young (<200 Ma) continental lithosphere, flexural rigidity is controlled by quartz-feldspathic rheology with a critical isotherm of ~350 °C and thus Fig. 13 cannot be directly compared to the values of elastic thickness.

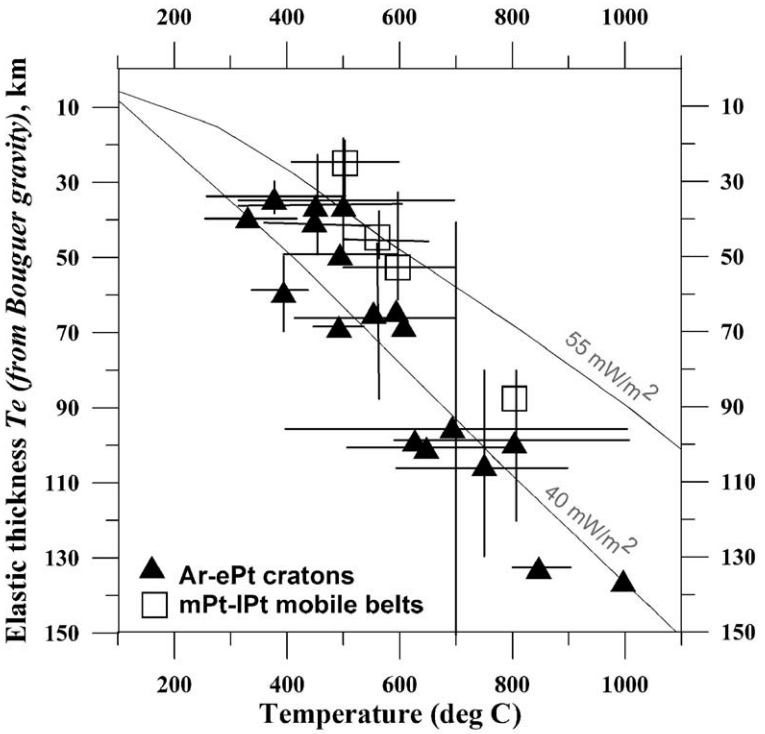

Fig. 14. Correlation between elastic thickness of Precambrian lithosphere (references are given in the text) and mantle temperatures derived from the TC1 model. Temperatures of 400–600 °C at the base of elastic lithosphere correspond to the brittle–ductile transition in mantle olivine. However, mechanism responsible for high T_e values (>70 km) associated with high mantle temperatures (600–850 °C) is unclear, which questions uniqueness of T_e constraints in some of the cratonic regions.

A comparison of thickness of elastic lithosphere (T_e) with mantle temperatures calculated in the present study indicates that the critical isotherm is between 400 and 600 °C (Fig. 14) for most of the cratons, where T_e values fall between 35 and 75 km (Archean–early Proterozoic Kaapvaal, Tanzania, and Slave cratons, Siberian platform, Baltic and Indian shields; middle–late Proterozoic Central Australia, Great Plains (USA) and Grenville province; Bechtel et al., 1990; Bhattacharji and Singh, 1984; Doucouré et al., 1996; Ebinger et al., 1989; Hartley and Allen, 1994; McKenzie and Fairhead, 1997; Poudjom Djomani et al., 1999; Petit and Ebinger, 2000; Pilkington, 1991; Simons et al., 2000). However, for the cratons with unusually large T_e values, 90–110 km (locally 130–140 km) (Superior province, Brazilian shield, East European Platform, Congo craton; Bechtel et al., 1990; Hartley et al., 1996; Kogan et al., 1994; Mantovani et al., 1995; Pilkington, 1991; Wang and Mareschal, 1999; Watts et al., 1995) the critical isotherm may be as high as 600–850 °C (Fig. 14). A discussion of the physical meaning of these high T_e values can be found in Watts (2001). Note that if the T_e depth in the Superior province, Brazilian shield, East European Platform, and the Congo craton corresponds to ~550–600 °C as favored by thermo-rheological models of the lithosphere, it would require that the thermal regime in these Archean–early Proterozoic terranes follows the reference geotherm of 30–35 mW/m^2.

7. Lithosphere growth and implications for the Archean–early Proterozoic tectonics

7.1. Growth rate of lithospheric mantle

The map of lithospheric thermal thickness for the continents (Fig. 12) was used (a) to evaluate the volume of the preserved continental lithosphere of different ages and (b) to calculate lithospheric growth rate since the Archean. Here continental lithosphere is defined as the area above sea level, and thus submerged areas with continental crust such as continental shelves and ocean plateaus are excluded from the analysis. Furthermore, it is assumed that the age of the crust is representative of the age of the underlying subcrustal lithosphere. Surface

Table 4
Present-day volume of the continental lithosphere of different ages

Age	Area (%)	Lithosphere volume ($\times 10^9$ km^3)	Lithosphere volume (%)	Total lithosphere volume (%)	Preserved crustal volume ($\times 10^8$ km^3)	Preserved crustal volume (in % of preserved lithosphere volume)
3.6–2.95 Ga (Ar)	11.2	4.24	15.3	15.3	9.20	21.7
2.95–2.55 Ga (Ar)	5.9	2.69	9.7	25.1	4.55	16.9
2.55–1.75 Ga (ePt)	12.1	4.55	16.5	41.6	10.50	23.1
1.75–1.15 Ga (mPt)	7.7	2.51	8.8	50.4	6.84	27.3
1.15 Ga–750 Ma (lPt)	9.4	2.38	8.6	59.0	7.47	31.4
750–550 Ma (lPt)	11.7	2.64	9.5	68.5	8.66	32.8
550–350 Ma (Pz)	12.0	2.62	9.4	77.9	8.48	32.4
350–0 Ma (Mz–Cz)	30.0	6.12	22.1	100	21.20	34.6
Total	100	27.75	99.9	–	76.90	27.7

area and volume of continental crust and lithosphere are calculated for spherical geometry at a 1°×1° grid using data on lithospheric thermal thickness interpolated by kriging on the same grid (Fig. 12). Data on crustal structure are derived from the CRUST 5.1 model (Mooney et al., 1998) and, for consistency, also interpolated on a 1°×1° grid. However, the crustal data were used solely to estimate the ratio of crustal to total volumes for the continental lithosphere. The results are summarized in Table 4.

Fig. 15(b) shows the growth rate of continental lithosphere over the past 3.6 Ga calculated with an age step of 200 and 300 Ma (Fig. 2). Although such a fine assignment of lithospheric ages is problematic in several continental regions (especially in platform areas with a thick sedimentary cover and an absence of accurate dating of basement rocks), it allows a rough comparison of lithospheric growth with global tectonic events, e.g., world-wide crust-forming events and superplumes (Fig. 15a).

The results suggest that the average growth rate of the continental lithosphere was ca. 5–8 km^3/year at 3.5–2.5 Ga, with a pronounced peak at 2.1–1.7 Ga when the growth rate became twice higher than in the Archean, and indicate that 50% of the present lithosphere was formed by 1.8 Ga. Assuming that juvenile crust comprised ca. 20–30% of juvenile lithosphere (Table 4), these results imply that crustal growth rate was ca. 1–1.5 km^3/year in the Archean and 2–3 km^3/year in early Proterozoic. These values are close to the estimates of average crustal growth rate in the Archean based on free-board and secular cooling constraints (Reymer and Schubert, 1984). Using Nd isotope data for North America, Greenland and the Baltic Shield, Patchett and Arndt (1986) calculated that the production rate of juvenile crust at 1.9 Ga was ca. 2.5 km^3/year. Similar values were obtained in many other studies. For example, Fig. 15c shows growth rate of juvenile crust calculated from the data of Abbott et al. (2000) and Condie (1998) with a time step of 100 Ma. I have chosen these two studies for a comparison because they are among the few, which indicate a non-monotonous crustal growth with the major crust-forming episodes at 2.7–2.5, 1.9–1.5, and 1.2–1.0 Ga.

There is a general agreement between the curves for the growth rate of the continental lithosphere and juvenile crust (Fig. 15b, c). However, note that all values of lithospheric volumes (crust plus lithospheric mantle) reported in this study refer to the *present-day* lithospheric volume which was preserved during the tectonic evolution of the continents, but not to the volume of the *juvenile* lithosphere. Thus, in fact, the curves for the "growth" rate of the continental lithosphere (Fig. 15b) reflect the cumulative effect of lithospheric growth and preservation and provide the lower limit for the curves of lithosphere growth. A comparison of Fig. 15b and c permits to speculate on tectonic evolution of the early continental lithosphere.

It is commonly accepted that the early juvenile crust was formed in Iceland-type plume-related tectonic settings (e.g., Ashwal et al., 1982) and in subduction zones (e.g., Abbott and Mooney, 1995). In the former case lithospheric mantle is produced by mantle differentiation simultaneously with the crust, while in the latter case this is not necessarily true. If the crust and the lithospheric mantle were produced by mantle differentiation, one would expect that a large volume of lithospheric mantle was generated at ca. 2.7 Ga during the peak in the production of juvenile crust (Fig. 15c). However, no significant peak in lithosphere volume is observed in the late Archean (Fig. 15b). Alternative explanations for the observed significant difference in the growth rate of *juvenile* crust and the growth rate of *preserved* lithosphere are: (a) a large portion of late Archean juvenile crust was formed in subduction zones without producing a significant

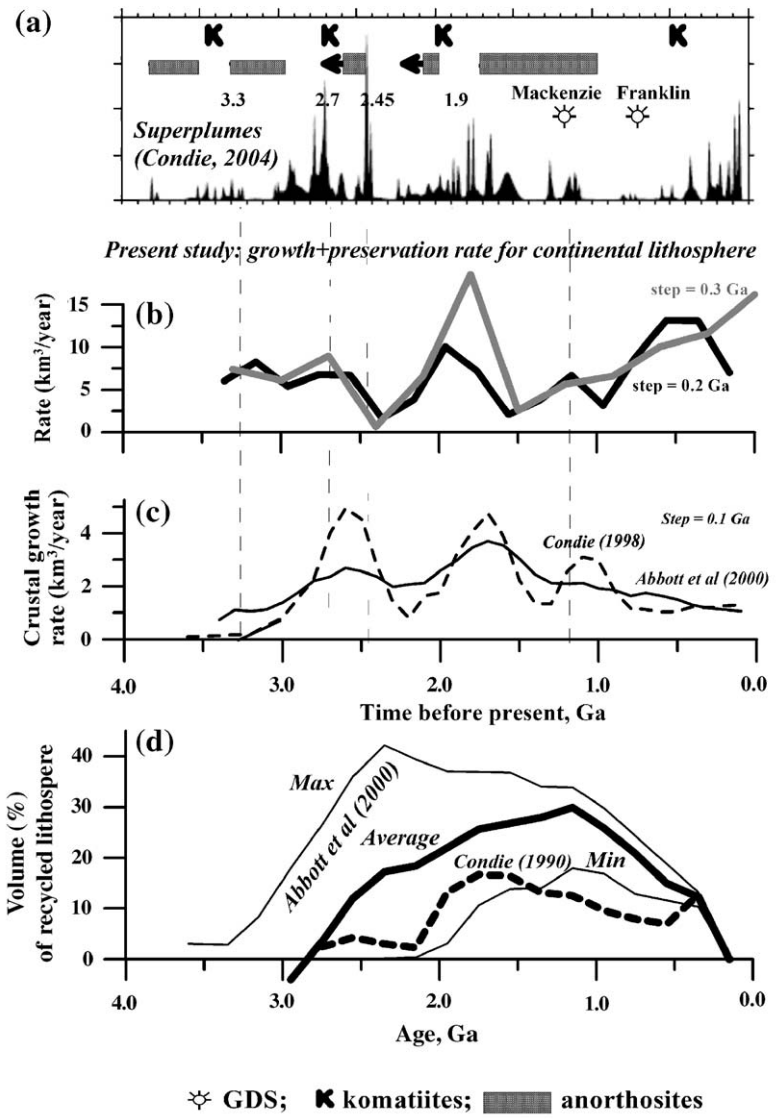

Fig. 15. Growth, preservation, and recycling of the continental lithosphere. (a) Timing of global tectonic events: superplumes, komatiite extraction, giant dike swarms (GDS) (after Condie, 2004, in press), and Archean and Proterozoic anorthosites (data from Ashwal, 1993). (b) Growth/preservation rate of the *present-day* continental lithosphere (crust + lithospheric mantle) calculated on a 1° × 1° grid from the global model of lithospheric thickness TC1 (Fig. 12) with age steps of 0.2 Ga (black line) and 0.3 Ga (gray line). The peak in lithospheric growth at ca. 1.7–2.0 Ga is a robust feature of the model. Note that this peak is followed by massive extraction of Proterozoic anorthosites suggesting that they were produced by edge-driven convection and not by mantle plumes. (c) Growth rate of the continental crust; dashed line—based on isotope ages of the juvenile crust (data from Condie, 1998); solid line—based on integrated interpretation of seismic data on the crustal structure and models of mantle melting (based on the average of the two models proposed by Abbott et al., 2000). Although there is a general agreement between Figures (b) and (c), the peak in the growth rate of juvenile crust at 2.7–2.5 Ga, associated with superplume events, is not evident in the curves of lithosphere growth/preservation. (d) Volume of recycled lithosphere calculated as the difference between the volume of *juvenile* lithosphere and the *present-day* volume of preserved continental lithosphere. The latter is based on the TC1 model. The former is derived from the volume of juvenile crust under an assumption that the ratio of juvenile crust to juvenile lithospheric mantle produced by mantle differentiation is constant through the geological history. Dashed line—calculated for age data from Condie, 1998; solid lines: "Max" calculated for the upper envelope of typical curves for the volume of juvenile crust (approximately the upper of the curves of McLennan and Taylor (1982) and Abbott et al. (2002)); "Min" calculated for the lower envelope (the lower of the curves of Abbott et al. (2002) and Veizer and Jansen (1985)); bold line is based on the average of the two models proposed by Abbott et al., 2000).

volume of juvenile lithospheric mantle; (b) most of the late Archean juvenile lithospheric mantle produced at ca. 2.7 Ga was delaminated (e.g., by a mechanism similar to flake tectonics (Hoffman and Ranalli, 1988)) and recycled back into the mantle. The latter possibility is examined further in this section.

Note, however, that a part of the discrepancy between the growth rates of juvenile crust and preserved lithosphere can be attributed to inaccuracy of the assigned ages. The assumptions used to constrain the age map for the lithosphere (Fig. 2) are discussed in detail in Section 2. Furthermore, most of the cratonic terranes contain a mixture of Archean and Proterozoic crust, and thus the actual volume of the Archean lithosphere is underestimated in this study, because the TC1 model is constrained by ages of the last major tectono-magmatic events when new material was added to the pre-existing juvenile lithosphere. Therefore, the older is a terrane, the larger can be an underestimate of its volume. On the other side, global statistics on the ages of juvenile crust can be biased by overrepresentation of North America, Baltica, and South Africa in isotope age data. For example, Nd analysis of Australian shales did not reveal any significant peaks in crustal growth rate at 3.3–0.2 Ga (Allègre and Rousseau, 1984) suggesting significant differences either in crustal growth or crustal recycling between different cratons.

Assuming that the ratio of *juvenile* crust to *juvenile* lithospheric mantle produced by mantle differentiation is constant throughout the geological evolution, the volume of juvenile crust (Fig. 15c) can be used to estimate the original volume of *juvenile* lithospheric mantle. The difference between the relative volumes of the crust and preserved lithospheric mantle can be interpreted as the volume of *recycled* lithosphere (Fig. 15d). The results suggest that, in the Archean, both the crust and the lithospheric mantle were recycled into the mantle at the same rate. Alternatively, they can be interpreted as indicating no recycling of the Archean lithospheric mantle older than 3.0 Ga and very limited recycling of the Archean lithosphere that is 3.0–2.0 Ga old, reflecting stabilization of cratonic lithosphere by the late Archean and its enhanced survivability with respect to mantle convection and tectonic processes. Another possibility proposed by Reymer and Schubert (1984) includes resetting of radiometric ages of early Archean juvenile crust during world-wide cratonization events at ca. 2.7 Ga, which could have led to the apparent high production rate of juvenile crust at that time (Fig. 15c), which is not reflected in the curves for lithosphere growth/preservation rate (based on thermo-tectonic ages, but not on isotope ages) (Fig. 15b).

7.2. Why do late Archean cratons have thick lithospheric roots?

The question of how the early lithosphere was formed remains enigmatic. A cogent evidence that plate tectonics operated already in the Archean is provided by recent seismic reflection studies across the margins of the Archean part of the Canadian Shield (e.g., Calvert et al., 1995; Cook et al., 1999) and by available paleomagnetic data. Numerous models of lateral and vertical growth of the continental nuclei can be reduced to (a) the "Iceland type" model of plume-induced mantle melting, further differentiation and magmatic underplating (e.g., Ashwal et al., 1982), and (b) collision of oceanic terranes, shallow subduction and underplating of slabs around the perimeters of pre-existing lithospheric fragments (Abbott and Mooney, 1995; Rudnick, 1995). These processes resulted in the existence of relatively large fragments of continental lithosphere already by 3.55–3.4 Ga as indicated by the wide-spread occurrence of metasediments with negative Eu anomalies (e.g., in Antarctica, Anabar shield in Siberia, Greenland) (Kröner, 1991).

A statistical analysis of age versus lithosphere thickness relationship for continents (Section 3) shows that, contrary to the expectations, the thickest lithosphere is identified beneath Archean cratons that are ca. 400–800 Ma younger than the oldest known cratonic terranes (>3.4 Ga, Fig. 4b and Table 2). The depth extent of cratonic lithosphere formed in the early Archean does not exceed ca. 200–220 km. Here, I propose that superthick (>250 km) cratonic roots with ages of 2.6–2.9 Ga were formed by Archean plate tectonic processes (i.e. during the assemblage of the cratons) and were not an immediate product of mantle differentiation as the "Iceland type" model implies.

A collision of continental nuclei with a 200–220 km thick lithosphere could led to tectonic stacking, lithosphere thrust-thickening and tectonic underplating, similar to the present-day Himalayas and Tibet, resulting in the formation of thick (60 km or more) crustal roots and superthick lithospheric roots. The preservation of such a thick crustal root requires that it was thermally insulated from the mantle by a thick lithospheric root. The lowermost part of the crust may later have transformed into eclogite facies and become seismically indistinguishable from the mantle. The lowermost part of an Archean lithospheric slab, despite its dry and depleted composition, could delaminate and recycle into the mantle in subduction settings (Lenardic et al., 2003), whereas its highly depleted devolatilised 250–350 km thick lithospheric root, formed at a paleo continent–

continent collision zone, could remain stable with respect to mantle convection and be preserved until present.

The lateral extent of superthick paleocollisional crustal and lithospheric roots can be relatively small (hundred to thousand kilometers) and restricted to the sutures between the Archean–early Proterozoic terranes. Because of their small size, such cratonic "teeth" would not necessarily be resolved in seismic models. However, they will be efficient in diverting heat from the mantle (Pollack, 1986) leading to low surface heat flow values at the site of a paleocollision. Unfortunately, surface heat flow measurements, sparse and uneven in many Archean terranes and sometimes restricted to regions of diamondiferous kimberlite fields (e.g., in Siberia), do not provide sufficient information on the lateral extent of superthick lithospheric roots. Moreover, it is possible that heat flow constraints on lithospheric geotherms in late Archean cratons (e.g., Siberia, Fennoscandia) are not globally (or even regionally) representative for terranes of that age. An alternative would be that most of the preserved late Archean cratons (3.0–2.5 Ga) have experienced significant plate tectonic interaction already in the Archean–early Proterozoic so that numerous thrust-thickened collisional belts were formed with

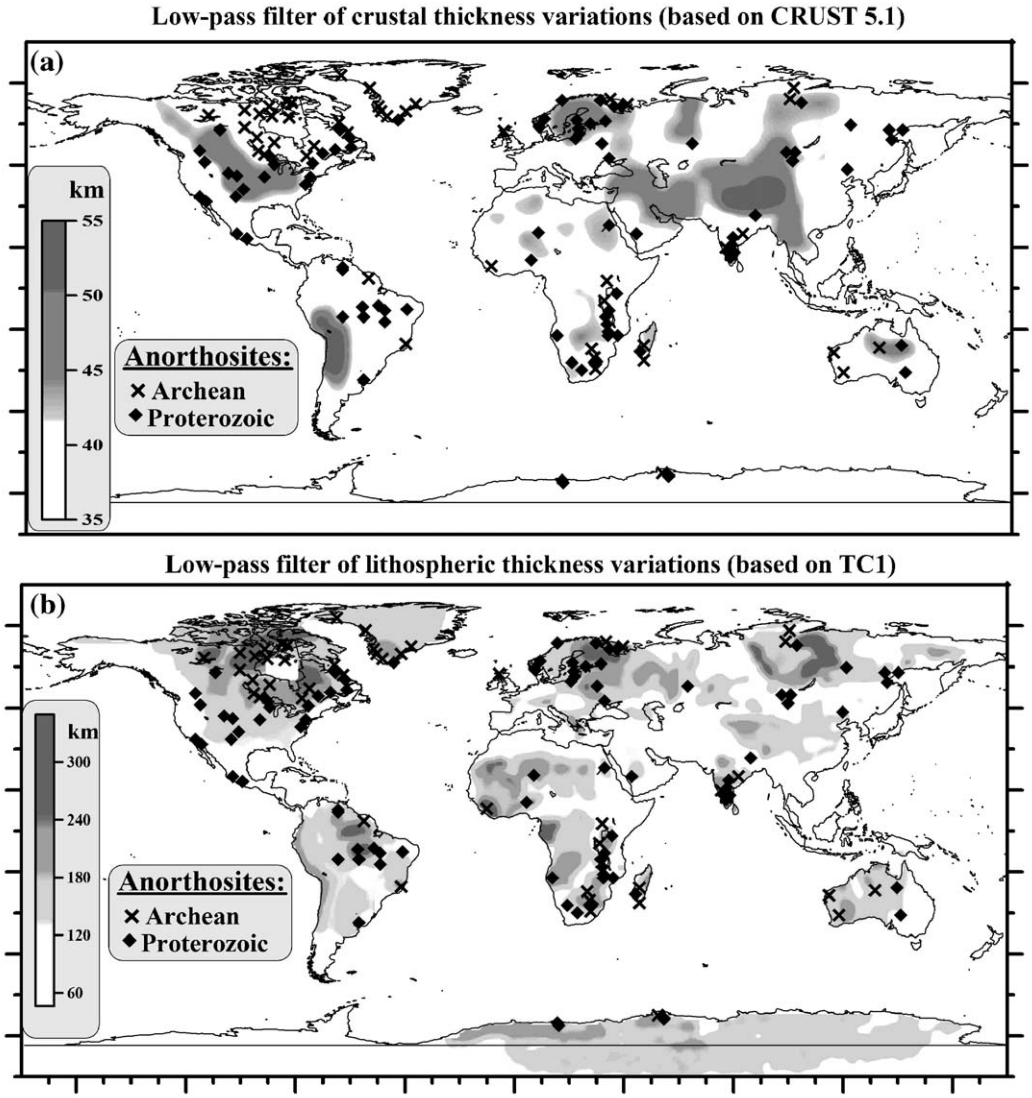

Fig. 16. Location of Precambrian AMGC complexes (data from Ashwal, 1993) superimposed on the maps of crustal thickness (a) and lithospheric thickness (b) variations. Proterozoic anorthosite belts are immediately adjacent to the areas with thick lithospheric roots and are located in the regions of thicker than normal (>42 km) Precambrian crust, everywhere where seismic data on the crustal structure exist.

several "lithospheric teeth" preserved within them until present. In such case seismic tomography would provide an integrated smoothed image of these "teeth" which can be interpreted as a single lithospheric keel. Zones of lithosphere weakness along the paleosutures and the presence of superthick "lithospheric teeth" would favor emplacement of diamond-bearing kimberlites within such cratons.

A belt of anorogenic magmatism (Proterozoic anorthosites or commonly associated with them granitoids including charnockites and rapakivi granites) can be another surface manifestation of a "lithospheric tooth". Some of Proterozoic anorthosites (e.g., central Finland, the Ukrainian Shield, southern India, central USA) were formed within cratonic interiors (Fig. 16); they could be produced by a deflection of a paleo-thermal anomaly in the mantle sidewards from the "lithospheric tooth".

The "diagnostic" features of "lithospheric teeth" can include a combination of: (i) a thick crustal root, (ii) low surface heat flow as compared to adjacent terranes, (iii) the presence of a paleo-suture or a paleo-orogen, and (iv) the presence of a belt of anorogenic magmatism at the edges of the "lithospheric tooth". Some of these features are observed, for example, in the Ukrainian shield, the Siberian Platform, and the Southern Granulite terrane in India, while all of them are observed in the Baltic Shield.

A region with some of the thickest known Precambrian crust, atypical for Archean cratons and locally reaching 60 km, is located at the boundary between the Archean Kola-Karelian and early Proterozoic Sveco-Fennian terranes in central Finland (Gorbatschev and Bogdanova, 1993). Mantle xenoliths from a kimberlite pipe at the terrane boundary indicate a cold cratonic geotherm (Fig. 6) and suggest the presence of a thick lithospheric root. This conclusion is further supported by the absence of shearing in xenoliths down to a 240 km depth (Kukkonen and Peltonen, 1999); high-temperature, sheared (and often metasomatised) peridotites are commonly interpreted as associated with mantle zones of reduced viscosity and asthenospheric flow. Low surface heat flow (30.2 ± 7.4 mW/m^2, $n = 16$) in the area suggests either an abnormally low-radiogenic crust, or a very thick lithospheric root, or a combination of both. A surface heat flow anomaly produced by a 300–350 km thick lithospheric root should have a wavelength of ca. 1000 km, in agreement with observations in Fennoscandia. Furthermore, the presence of rapakivi granites encircling the region with the thick crust and low surface heat flow from north, west and south provides further support for the proposed process and the presence of a superthick lithospheric tooth (250–300 km) with a limited lateral extent.

8. Lithospheric structure and middle Proterozoic anorthosites

I propose that the structure of the continental lithosphere has controlled anorogenic magmatism and, in particular, the extraction of Precambrian anorthosites (igneous rocks containing >90% of plagioclase, many of them being metamorphosed). Geological and geochemical data on Precambrian anorthosites used in further discussion are based on an excellent compilation of Ashwal (1993).

Archean megacrystic anorthosites, which have distinctive geochemical characteristics, are associated with mafic melts and flows of basaltic composition and are found at different tectonic settings within the Archean terranes. Presumably they were formed within oceanic crustal environments. Archean anorthosites are more common in cratons of the northern hemisphere than of the southern hemisphere (Ashwal, 1993). This accords with the results of the thermal modeling which indicate that Archean cratons with thick lithospheric roots (>250 km) are restricted chiefly to the northern hemisphere, while the lithosphere in Archean cratons of the southern hemisphere is much thinner (ca. 200 km) (Artemieva and Mooney, 2001, 2002). Furthermore, a comparison of Figs. 12 and 16b indicates that many Archean anorthosites are located at the edges of Archean terranes with thick lithospheric roots.

Conversely, the most voluminous and abundant, massif-type anorthosites are almost uniquely a middle-Proterozoic phenomenon (Ashwal, 1993). They are formed by intrusive complexes, which typically are not associated with large volumes of mafic or ultramafic rocks and are restricted in time and space (Ashwal, 1993 and Figs. 15a, 16). Although Proterozoic anorthosites formed over a 600 Ma time span, most of them were emplaced at 1.85–1.55 and 1.35–1.15 Ga (compare with Fig. 15b, which shows peaks in lithospheric growth at this time). Plotted on paleo-continental reconstructions, massif-type anorthosites appear to group into two "belts": one across Laurasia and the other one across the Gondwana continents. Proterozoic granitoids (including charnockites and rapakivi granites) are commonly associated with massif-type anorthosites and many of them are distributed along the Laurasian anorthosite belt (c.f. Ashwal, 1993), although petrogenetic links between them are debated. Proterozoic anorthosites are believed to be a product of basaltic, ultramafic, or anorthositic magmatism, many of them were significantly contaminated with the crustal material.

Although different tectonic settings have been proposed for petrogenesis of massif-type anorthosites, none

of them can entirely explain their differentiation, crystallization, and metamorphic history. Moreover, most of the hypotheses fail to explain why massif-type anorthosites are a uniquely Proterozoic phenomenon. An exception is the model of Hoffman (1989) which proposes that Proterozoic anorthosites were formed after an early Proterozoic assemblage of Archean microcontinents into a supercontinent (Laurentia); thermal blanketing of convective mantle by continental lithosphere produced a mantle superswell and wide-spread anorogenic magmatism. As pointed out by Ashwal (1993), this model fails to explain why Proterozoic anorthosites within the Superior craton are so scarce and why a superswell did not cause a supercontinent break-up.

I next propose a genetic link between lithospheric growth and anorthosite formation in middle Proterozoic based on (i) the correlation between the spatial distribution of Proterozoic anorthosites and lithospheric structure (Fig. 16) and (ii) on the correlation between the time of their extraction and lithosphere growth rate (Fig. 15 a, b). I advocate that large-scale variations in lithospheric thickness at cratonic margins and at paleoterrane boundaries controlled the extraction of Precambrian anorthosites. It is outside the scope of this study to consider geochemical arguments for or against the proposed hypothesis.

Fig. 15b shows that for the post-Archean lithosphere, the major peak in the rate of lithospheric growth correlates with one of the major world-wide recognized crust-forming episodes at 2.0–1.7 Ga (e.g., Reymer and Schubert, 1987). These peaks in crustal and lithospheric growth are followed by a global extraction of Proterozoic massif-type anorthosites (Fig. 15a). I hypothesize that they were produced by vigorous small-scale convection at the margins of continental lithospheric keels formed at 2.0–1.7 Ga, similarly to the mechanism proposed by King and Anderson (1995) for a formation of large igneous provinces. Fig. 16b demonstrates that middle Proterozoic belts of anorogenic magmatism are more abundant at the edges of the cratons with exceptionally thick lithospheric roots. Besides, everywhere where seismic data on the crustal structure exist, Proterozoic anorthosites are concentrated in the regions of thicker than normal (>42 km) Precambrian crust (Fig. 16a).

Ashwal (1993) pointed out that many middle-Proterozoic massif-type anorthosites were emplaced at terrane boundaries, for example, at the Grenville front and the Nain–Churchill boundary in Labrador, at the edge of the Eastern Ghats in India, at the western margin of the East European Platform, along the margins of the Kola Peninsula, or along the southern margin of the Aldan shield (the Stanovoy Ridge). Note that all of these tectonic settings are marked by a pronounced step in lithospheric thickness (Figs. 12, 16b), typically ca. 50–75 km over a lateral distance of 200–600 km. Steady-state thermal modeling does not permit to distinguish smaller-scale variations in lithospheric structure, which are masked by a horizontal component of conductive heat transfer in the lithosphere.

Similar to Archean anorthosites, more massif-type anorthosites are known in the northern than in the southern hemisphere; they are not abundant in South America and Africa and are not known at all in Australia (Ashwal, 1993). This can be a consequence of a significant difference in lithospheric growth rates on the cratons of the two hemispheres. While model Nd ages of basement rocks cluster around 1.9–1.7 Ga in North America (e.g., Nelson and DePaolo, 1985) suggesting high rates of crustal growth at that time, Nd analysis of shales from Australia did not indicate any significant peaks in crustal growth rate at 1.9–1.7 Ga (Allègre and Rousseau, 1984).

9. Conclusions

Surface heat flow measurements allow us to constrain the thermal state of the upper mantle only for about 40% of the continents, which is sufficient to perform a statistically significant analysis of lithospheric geotherms for continental terranes with different tectonic settings and different geological ages. New compilation of crustal ages (Fig. 2) together with previously reported geotherms for stable continental regions (Artemieva and Mooney, 2001) form the basis for this analysis. These data were supplemented by xenolith P–T arrays and electrical conductivity profiles for cratonic regions. A major assumption for the analysis is that lithospheric mantle has the same age as the overlying crust. A new global thermal model TC1 for the continental lithosphere is constrained on a $1° \times 1°$ grid.

The following conclusions are made from the study.

1) Xenolith P–T arrays confirm the results of the thermal model and suggest that there are two groups of Archean cratons with significantly different thermal regimes. Cratons with lower mantle temperatures follow a ca. 35–38 mW/m^2 conductive geotherm and include Archean terranes of the northern hemisphere (Slave craton, Fennoscandia (central Finland and Arkhangelsk region), and Siberia). Xenolith P–T arrays for Kaapvaal, Namibia, Superior and Wyoming cratons, and Somerset Island follow a 40–45 mW/m^2 conductive geotherm. The difference between the 37 and 42 mW/m^2 geotherms implies ca. 80–100 km difference in the lithospheric thickness

between the cratons in the two groups. Depth curves of electrical conductivity, which are surprisingly similar for all cratons, further support the conclusion that conductive geotherms between 35 and 50 mW/m^2 are characteristic of all of the Archean cratons.

2) Statistical analysis of lithospheric geotherms reveals a striking correlation (r=0.94) between the age of terranes and their thermal regime: the lithospheric thermal thickness linearly decreases with time from Mesoarchean to present. However, this correlation can be biased by the uneven distribution of heat flow measurements as indicated by the lower value of area-weighted correlation (r=0.68) calculated on a 1°×1° grid.
3) Contrary to the global trend, lithosphere is thicker in young Archean than in old Archean (>3.0 Ga) cratons. Thick lithospheric roots (250–350 km) are found solely for 3.0–2.5 Ga old cratons. In several Archean cratons regions with low heat flow, thick crust and thick lithosphere spatially coincide with paleoterrane boundary(ies). I propose that in such regions an exceptionally thick lithosphere has a relatively small lateral extent and was formed during Archean–early Proterozoic thrust-thickening collisions of pre-existing continental nuclei. Heat from the mantle during episodes of high tectonic activity could be effectively diverted by such "lithospheric teeth", forming belts of anorogenic magmatism at their edges.
4) The strong correlation between the thermal state and the age of the lithosphere allows us to build a new global thermal model TC1 of the continental lithosphere on a 1°×1° grid, which shows strong thermal heterogeneity of the continental mantle. Maximum temperature anomalies (up to 800 °C) in shallow mantle can produce seismic velocity anomalies of up to 3%. A map of the depth to the 550 °C isotherm provides a proxy for the thickness of the magnetic crust and for the thickness of a mechanically strong layer in >200 Ma old lithosphere with olivine rheology of the mantle.
5) A new global map of lithospheric thickness, constrained by the TC1 model, was used to estimate the volume of the preserved continental lithosphere, which is ca. 27.8 (±7.0)×10^9 km^3 (excluding submerged terranes with continental crust such as oceanic plateaus and shelves). The average growth rate of the continental lithosphere was ca. 5–8 km^3/year in the Archean and twice higher at 2.1–1.7 Ga. About 50% of the present continental lithosphere was formed by 1.8 Ga.
6) The growth rate of the lithosphere since the Archean (as manifested by its present-day lithospheric volume for terranes of different ages) does not reveal a peak in lithospheric volume at 2.7–2.6 Ga as expected from growth curves for juvenile crust. A nearly zero rate of lithosphere recycling was calculated for the Archean–early Proterozoic lithosphere, reflecting stabilization of cratonic lithosphere by the late Archean and its enhanced survivability.
7) The major peak in the rate of lithospheric growth correlates with one of the major world-wide recognized crust-forming episodes at 2.0–1.7 Ga and is followed by a global extraction of Proterozoic massif-type anorthosites. I propose that large-scale variations in lithospheric thickness at cratonic margins and at paleoterrane boundaries controlled anorogenic magmatism and, in particular, the extraction of Precambrian anorthosites which were produced by vigorous small-scale convection at the margins of continental lithospheric keels formed at 2.0–1.7 Ga. The hypothesis is based on the observed correlations (a) between the spatial distribution of Proterozoic anorthosites and lithospheric structure and (b) between the time of their extraction and lithosphere growth rate. More common and more voluminous occurrence of middle Proterozoic massive anorthosites in the northern hemisphere (where xenolith and thermal data suggest an exceptionally thick cratonic lithosphere) supports the hypothesis that their emplacement can be associated with a presence of >250 km lithospheric roots.

Acknowledgements

Constructive thoughtful reviews of Dallas Abbott, Kent Condie and Jean-Claude Mareschal are gratefully acknowledged. The study was supported by a personal research grant from the Carlsbergfondet, Denmark. Digital files for the TC1 model can be downloaded from: www.lithosphere.info.

References

Abbott, D., Mooney, W.D., 1995. The structural and geochemical evolution of the continental crust: support for the oceanic plateau model of continental growth. Rev. Geophys., Suppl. 231–242.

Abbott, D.H., Burgess, L., Longhi, J., Smith, W.H.F., 1994. An empirical thermal history of the earth's upper mantle. J. Geophys. Res. 99, 13835–13850.

Abbott, D., Sparks, D., Herzberg, C., Mooney, W., Nikishin, A., Zhang, Y.Sh., 2000. Quantifying Precambrian crustal extraction: the root is the answer. Tectonophysics 322, 163–190.

Adam, A., 1976. Quantitative connections between regional heat flow and the depth of conductive layers in the earth's crust and upper mantle. Acta. Geodeat. Geophys. et Montanist. Acad. Sci. Hung. 11, 503–509.

Adam, A., Wesztergom, V., 2001. An attempt to map the depth of the electrical asthenosphere by deep magnetotelluric measurements in the Pannonian Basin (Hungary). Acta Geol. Hung. 44, 167–192.

Allègre, C.J., Rousseau, D., 1984. The growth of the continents through geological time: studies by Nd isotope analysis of shales. Earth Planet. Sci. Lett. 67, 19–34.

Artemieva, I.M., Mooney, W.D., 2001. Thermal structure and evolution of Precambrian lithosphere: a global study. J. Geophys. Res 106, 16387–16414.

Artemieva, I.M., Mooney, W.D., 2002. On the relation between cratonic lithosphere thickness, plate motions, and basal drag. Tectonophysics 358, 211–231.

Artemieva, I.M., Billien, M., Lévêque, J.-J., Mooney, W.D., 2004. Shear-wave velocity, seismic attenuation, and thermal structure of the continental upper mantle. Geophys. J. Int. 157, 607–628.

Aschepkov, I., Vladykin, N., Pokhilenko, N., et al., 2003. Clinopyroxene geotherms for the mantle columns beneath kimberlite pipes from Siberian craton. Proc. 8th Intern. Kimberlite Conf., Victoria, BC, Canada, June 2003: FLA-0355.

Ashwal, L.D., 1993. Anorthosites. Springer-Verlag, Berlin. 366 pp.

Ashwal, L.D., Phinney, W.C., Morrison, D.A., Wooden, J.L., 1982. Underplating of Archean continents: evidence from the Bad Vermilion Lake anorthosite complex, Ontario. Lunar Planet. Sci. 13, 20–21.

BABEL Working Group, 1993. Deep seismic reflection/refraction interpretation of crustal structure along BABEL profiles A and B in the southern Baltic Sea. Geophys. J. Int. 112, 325–343.

Bahr, K., 1985. Magnetotellurische Messung des Elektrischen Widerstandes der Erdkruste und des Oberen Mantels in Gebieten mit Lokalen und Regionalen Leitfahigkeitsanomalien. PhD thesis, Univ. Gottingen.

Bassin, C., Laske, G., Masters, G., 2000. The current limits of resolution for surface wave tomography in North America. EOS Trans. AGU 81, F897.

Bechtel, T.D., Forsyth, D.W., Sharpton, V.L., Grieve, R.A.F., 1990. Variations in effective elastic thickness of the North American lithosphere. Nature 343, 636–638.

Berdichevsky, M.N., Vanyan, L.L., Kuznetsov, V.A., Levadny, V.T., Mandelbaum, M.M., Nechaeva, G.P., Okulessky, B.A., Shilovsky, P.P., Shpak, I.P., 1980. Geoelectric model of the Baikal region. Phys. Earth Planet. Int. 22, 1–11.

Bhattacharji, S., Singh, R.N., 1984. Thermal mechanical structure of the southern part of the Indian Shield and its relevance to Precambrian basin evolution. Tectonophysics 105, 103–120.

Boyd, F.R., 1984. Siberian geotherm based on lherzolite xenoliths from Udachnaya kimberlite, USSR. Geology 12, 528–530.

Boyd, F.R., Gurney, J.J., 1986. Diamonds and the African lithosphere. Science 232, 472–477.

Boyd, F.R., Fujii, T., Danchin, R.V., 1976. A noninflected geotherm for the Udachnaya kimberlite pipe, USSR. Carnegie Year Book 1975, pp. 523–531.

Brey, G., Köhler, T., Nickel, K.G., 1990. Geothermobarometry in four-phase lherzolites: I. Experimental results from 10 to 60 kb. J. Petrol. 31, 1313–1352.

Calvert, A.J., Sawyer, E.W., Davis, W.J., Ludden, J.N., 1995. Archean subduction inferred from seismic images of a mantle suture in the Superior province. Nature 375, 670–674.

Clowes, R.M., Cook, F.A., Ludden, J.N., 1998. LITHOPROBE leads to new perspectives on continental evolution. GSA Today 8, 1–7.

Coisy, P., Nicolas, A., 1978. Regional structure and geodynamics of the upper mantle beneath the Massif Central. Nature 274, 429–432.

Condie, K.C., 1998. Episodic continental growth and supercontinents: a mantle avalanche connection? Earth Planet Sci. Lett. 163, 97–108.

Condie, K.C., 2001. Mantle Plumes and their Record in Earth History. Cambridge Univ. Press. 306 pp.

Condie, K.C., 2005. Earth as an Evolving Planetary System. Elsevier. 359 pp.

Constable, S., Shankland, T.J., Duba, A., 1992. The electrical conductivity of an isotropic olivine mantle. J. Geophys. Res. 97, 3397–3404.

Cook, F.A., van der Velden, A.J., Hall, K.W., Roberts, B.J., 1999. Frozen subduction in Canada's Northwest Territories: LITHOPROBE deep lithospheric reflection profiling of the western Canadian shield. Tectonics 18, 1–26.

Deschamps, F., Trampert, J., Snieder, R., 2002. Anomalies of temperature and iron in the uppermost mantle inferred from gravity data and tomographic models. Phys. Earth Planet. Int. 129, 245–264.

Dobson, D.P., Brodholt, J.P., 2000. The electrical conductivity and thermal profile of the earth's mid-mantle. Geophys. Res. Lett. 27, 2325–2328.

Doin, M.-P., Fleitout, L., Christensen, U., 1997. Mantle convection and stability of depleted and undepleted continental lithosphere. J. Geophys. Res. 102, 2771–2787.

Doucouré, C.M., de Wit, M.J., Mushayandebvu, M.F., 1996. Effective elastic thickness of the continental lithosphere in South Africa. J. Geophys. Res. 101, 11291–11303.

Dunn, D., Smith, D., Bergman, S.C., 2003. Mantle xenoliths from the Prairie Creek Lamproite Province, Arkansas, USA. Proc. 8th Intern. Kimberlite Conf., Victoria, BC, Canada, June 2003: FLA-0119.

Ebinger, C.J., Bechtel, T.D., Forsyth, D.W., Bowin, C.O., 1989. Effective elastic plate thickness beneath the East African and Afar plateaus and dynamic compensation of the uplifts. J. Geophys. Res. 94, 2883–2901.

Eggler, D.H., Meen, J.K., Welt, F., Dudas, F.O., Furlong, K.P., McCallum, M.E., Carlson, R.W., 1988. Tectonomagmatism of the Wyoming Province. Cenozoic volcanism in the southern Rocky Mountains revisited; a tribute to Rudy C. Epis: Part 3. Colorado School of Mines Quarterly, vol. 83, No. 2, pp. 25–40.

Engelhardt, H., 2004. Ice temperature and high geothermal flux at Siple Dome, west Antarctica, from borehole measurements. J. Glaciol. 50 (169), 251–256.

ERCEUGT-Group, 1992. An electrical resistivity crustal section from the Alps to the Baltic Sea (central segment of the EGT). Tectonophysics 207, 123–139.

Finnerty, A.A., Boyd, F.R., 1987. Thermobarometry for garnet peridotites: basis for the determination of thermal and compositional structure of the upper mantle. In: Nixon, P.H. (Ed.), Mantle Xenoliths. Wiley and Sons, pp. 381–402.

Fitzgerald, P., 2002. Tectonics and landscape evolution of the Antarctic plate since the breakup of Gondwana, with an emphasis on the west Antarctic rift system and the transantarctic mountains. Antarctica at the close of a millenium. R. Soc. NZ Bull. 35, 453–469.

Forte, A.M., Woodward, R.L., Dziewonski, A.M., 1994. Joint inversions of seismic and geodynamic data for models of three-dimensional mantle heterogeneity. J. Geophys. Res. 99, 21857–21887.

Freybourger, M., Gaherty, J.B., Jordan, T.H., Kaapvaal Seismic Group, 2001. Structure of the Kaapvaal craton from surface waves. Geophys. Res. Lett. 28, 2489–2493.

Furlong, K.P., Spakman, W., Wortel, R., 1995. Thermal structure of the continental lithosphere—constraints from seismic tomography. Tectonophysics 244 (1–3), 107–117.

Godey, F., Deschamps, J., Trampert, R., Snieder, R., 2004. Thermal and compositional anomalies beneath the North American continent. J. Geophys. Res. 109, B01308. doi:10.1029/2002JB002263.

Goodwin, A.M., 1996. Principles of Precambrian Geology. Academic Press, London. 327 pp.

Gorbatschev, R., Bogdanova, S., 1993. Frontiers in the Baltic Shield. Precambrian Res. 64, 3–21.

Griffin, W.L., Sobolev, N.V., Ryan, C.G., Pohkilenko, N.P., Win, T.T., Yefimova, E.S., 1993. Trace elements in garnets and chromites: diamond formation in the Siberian lithosphere. Lithos 29, 235–256.

Griffin, W.L., Kaminsky, F.V., Ryan, C.G., O'Reilly, S.Y.O., Win, T.T., Ilupin, I.P., 1996. Thermal state and composition of the lithospheric mantle beneath the Daldyn kimberlite field, Yakutia. Tectonophys 262, 19–33.

Griffin, W.L., O'Reilly, S.Y., Ryan, C.G., Gaul, O., Ionov, D.A., 1998a. Secular variation in the composition of subcontinental lithospheric mantle: geophysical and geodynamic implications. AGU Geodynam. Monograph 26, 1–26.

Griffin, W.L., Andi, Z., O'Reilly, S.Y., Ryan, C.G., 1998b. Phanerozoic evolution of the lithosphere beneath the Sino–Korean craton. Mantle Dynamics and Plate Interactions in East Asia AGU Geodynam. Monogr., vol. 27, pp. 107–126.

Griffin, W.L., Ryan, C.G., Kaminsky, F.V., O'Reilly, S.Y., Natapov, L. M., Win, T.T., Kinny, P.D., Ilupin, I.P., 1999. The Siberian lithosphere traverse; mantle terranes and the assembly of the Siberian craton. Tectonophysics 310, 1–35.

Griffin, W.L., O'Reilly, S.Y., Doyle, B.J., Kivi, K., Coopersmith, H.G., 2003. Lithospheric mapping beneath the North American Plate. Proc. 8th Intern. Kimberlite Conf., Victoria, BC, Canada, June 2003.

Grutter, H.S., Moore, R.O., 2003. Pyroxene geotherms revisited—an empirical approach based on Canadian xenoliths. Proc. 8th Intern. Kimberlite Conf., Victoria, BC, Canada, June 2003: FLA-0272.

Hartley, R., Allen, P.A., 1994. Interior cratonic basins of Africa: relation to continental break-up and role of mantle convection. Basin Res. 6, 95–113.

Hartley, R., Watts, A.B., Fairhead, J.D., 1996. Isostasy of Africa. Earth Planet. Sci. Lett. 137, 1–18.

Hearn Jr., B.C., 2003. Upper-mantle xenoliths in the homestead Kimberlite, central Montana, USA: depleted and re-enriched Wyoming craton samples. Proc. 8th Intern. Kimberlite Conf., Victoria, BC, Canada, June 2003: FLA-0126.

Hjelt, S.E, Korja, T., 1993. Lithospheric and upper-mantle structures, results of electromagnetic soundings in Europe. Phys. Earth Planet. Int. 79 (1–2), 137–177.

Hoffman, P.F., 1989. Speculations on Laurentia's first gigayear (2.0 to 1.0 Ga). Geology 17, 135–138.

Hoffman, P.F., Ranalli, G., 1988. Archean oceanic flake tectonics. Geophys. Res. Lett. 15, 1077–1080.

Ionov, D.A., O'Reilly, S.Y., Griffin, W.L., 1998. A geotherm and lithospheric section for central Mongolia (Tariat region). In: Flower, M., Chung, S.L., Lo, C.H., Lee, T.Y. (Eds.), Mantle Dynamics and Plate Interactions in East Asia American Geophysical Union, Washington D.C. Geodynamics, vol. 27, pp. 127–154.

Jackson, I., 2000. Laboratory measurement of seismic wave dispersion and attenuation: recent progress. Geophys. Monogr. 117, 265–289.

Jones, A.G., 1999. Imaging the continental upper mantle using electromagnetic methods. Lithos 48, 57–80.

Jones, A.G., Lezaeta, P., Ferguson, I.J., Chave, A.D., Evans, R.L., Garcia, X., Spratt, J., 2003. The electrical structure of the Slave craton. Lithos 71, 505–527.

Kampfmann, W., Berckhemer, H., 1985. High temperature experiments on the elastic and anelastic behaviour of magmatic rocks. Phys. Earth Planet. Int. 40, 223–247.

Karato, S., 1990. The role of hydrogen in the electrical conductivity of the upper mantle. Nature 357, 272–273.

Kennedy, C.S., Kennedy, G.C., 1976. The equilibrium boundary between graphite and diamond. J. Geophys. Res. 81, 2467–2470.

King, S.D., Anderson, D.L., 1995. An alternative mechanism of flood basalt formation. Earth Planet. Sci. Lett. 136, 269–279.

Kohlstedt, D.L., Evans, B., Mackwell, S.J., 1995. Strength of the lithosphere: constraints imposed by laboratory experiments. J. Geophys. Res. 100, 17587–17602.

Kogan, M.G., Fairhead, J.D., Balmino, G., Makedonskii, E.L., 1994. Tectonic fabric and lithospheric strength of northern Eurasia based on gravity data. Geophys. Res. Lett. 21, 2653–2656.

Kopylova, M.G., Caro, 2001. Proc. Slave–Kaapvaal Workshop, Merrickville, Canada, Sept. 5–9, 2001. www.cg.nrcan.gc.ca/slave–kaapvaal-workshop/2001.

Kopylova, M.G., McCammon, C., 2003. Composition and the redox state of the Slave peridotitic mantle. Proc. 8th Intern. Kimberlite Conf., Victoria, BC, Canada, June 2003: FLA-0195.

Kopylova, M.G., Russell, J.K., Cookenboo, H., 1999. Petrology of peridotite and pyroxenite xenoliths from the Jericho kimberlite: implications for the thermal state of the mantle beneath the Slave craton, northern Canada. J. Petrol. 40, 79–104.

Korja, T., 1993. Electrical conductivity distribution of the lithosphere in the central Fennoscandian Shield. Precambrian Res. 64, 85–108.

Korja, T., Engels, M., Zhamaletdinov, A.A., et al., 2002. Crustal conductivity in Fennoscandia—a compilation of a database on crustal conductance in the Fennoscandian Shield. Earth Planets Space 54 (5), 535–558.

Kröner, A., 1991. Tectonic evolution in the Archaean and Proterozoic. Tectonophys 187, 393–410.

Kuge, K., Fukao, Y., 2005. High-velocity lid of east Antarctica: evidence of a depleted continental lithosphere. J. Geophys. Res. 110, B06309. doi:10.1029/2004JB003382.

Kukkonen, I.T., Peltonen, P., 1999. Xenolith-controlled geotherm for the central Fennoscandian Shield: implications for lithosphere–asthenosphere relations. Tectonophys 304, 301–315.

Kurtz, R.D., Craven, J.A., Niblett, E.R., Stevens, R.A., 1993. The conductivity of the crust and mantle beneath the Kapuskasing Uplift: electrical anisotropy in the upper mantle. Geophys. J. Int. 113, 483–498.

Kusznir, N., Karner, G., 1985. Dependence of the flexural rigidity of the continental lithosphere on rheology and temperature. Nature 316, 138–142.

Laske, G., Master, s.G., 1997. A global digital map of sediment thickness. EOS Trans. AGU 78, F483.

Le Bas, M.J., 1987. Ultra-alkaline magmatism with or without rifting. Tectonophys 143, 75–84.

Ledo, J., Jones, A.G., 2005. Upper mantle temperature determined from combining mineral composition, electrical conductivity laboratory studies and magnetotelluric field observations:

application to the intermontane belt, northern Canadian Cordillera. Earth Planet. Sci. Lett. 236, 258–268.

Lee, C.-T., Rudnick, R.L., 1999. Compositionally stratified cratonic lithosphere: petrology and geochemistry of peridotite xenoliths from the Labait tuff cone, Tanzania. In: Gurney, J.J., Richardson, S.R. (Eds.), Proc. 7th Int. Kimberlite Conference, Red Roof Designs, Cape Town, pp. 503–521.

Lehtonen, M.L., OBrien, H.E., Peltonen, P., Johanson, B.S., Pakkanen, L.K., 2003. Layered mantle at the edge of the Karelian craton: *P–T* of mantle xenocrysts and xenoliths from eastern Finland kimberlites. Proc. 8th Intern. Kimberlite Conf., Victoria, BC, Canada, June 2003: FLA-0260.

Lenardic, A., Moresi, L.N., Muhlhaus, H., 2003. Longevity and stability of cratonic lithosphere: insights from numerical simulations of coupled mantle convection and continental tectonics. J. Geophys. Res. 108 (B6), 2303. doi:10.1029/2002JB001859.

Litasov, K.D., Litasov, Y.D., Malkovets, V.G., Taniguchi, H., 2003. Lithosphere structure and thermal regime of the upper mantle beneath the Baikal Region: evidence from deep-seated xenoliths. Proc. 8th Intern. Kimberlite Conf., Victoria, BC, Canada, June 2003: FLA-0030.

Lucazeau, F., Brigaud, F., Bouroullec, J.L., 2004. High-resolution heat flow density in the lower Congo basin. Geochem. Geophys. Geosyst. 5, Q03001. doi:10.1029/2003GC000644.

MacGregor, I.D., 1974. The system MgO–Al_2O_3–SiO_2: solubility of Al_2O_3 in enstatite for spinel and garnet peridotite compositions. Am. Mineral. 59, 110–119.

Malkovets, V.G., Taylor, L.A., Griffin, W., O'Reilly, S., Pearson, N., Pokhilenko, N.P., Verichev, E.M., Golovin, N.N., Litasov, K.D., 2003. Cratonic conditions beneath Arkhangelsk, Russia: garnet peridotites from the Grib kimberlite. Proc. 8th Intern. Kimberlite Conf., Victoria, BC, Canada, June 2003: FLA-0220.

Mantovani, E., Albarello, D., Tamburelli, C., Viti, M., 1995. Tectonic interpretation of large scale geodetic measurements (VLBI, SLR) in the central Mediterranean region; constraints and uncertainties. Ann. Geofis. 38 (1), 67–84.

Mareschal, M., Kellet, tR.L., Kurtz, R.D., Ludden, J.N., Ji, S., Balley, R.C., 1995. Archaean cratonic roots, mantle shear zones and deep electrical anisotropy. Nature 375, 134–137.

Masse, P., 1983. The possible relations between grabens, wrench faults and uplifting in the intracontinental rifts. In: Popoff, M., Tiercelin, J. (Eds.), Rifts et Fosse's AnciensBull. Cent. Rech. Explor.-Prod. Elf-Aquitaine, vol. 7, pp. 149–154.

Maule, C.F., Purucker, M.E., Olsen, N., et al., 2005. Heat flux anomalies in Antarctica revealed by satellite magnetic data. Science 309 (5733), 464–467.

McKenzie, D., Fairhead, D., 1997. Estimates of the effective elastic thickness of the continental lithosphere from Bouguer and free air gravity anomalies. J. Geophys. Res. 102, 27523–27552.

Menzies, A.H., Westerlund, K., Gurney, J.J., Carlson, J., Fung, A., Nowicki, T., 2003. Peridotitic mantle xenoliths from kimberlites on the Ekati Diamond Mine Property, NWT, Canada. Proc. 8th Intern. Kimberlite Conf., Victoria, BC, Canada, June 2003: FLA-0305.

Mooney, W.D., Laske, G., Masters, G., 1998. CRUST 5.1: a global crustal model at 5° × 5°. J. Geophys. Res. 103, 727–747.

Moroz, Y.F., Pospeev, A.V., 1985. Deep electrical conductivity of east Siberia and the Far East of Russia. Tectonophys 245, 85–92.

Neal, S.L., Mackie, R.L., Larsen, J.C., Schultz, A., 2000. Variations in the electrical conductivity of the upper mantle beneath North America and the Pacific Ocean. J. Geophys. Res. 105, 8229–8242.

Nelson, B.K., DePaolo, D.J., 1985. Rapid production of continental-crust 1.7 to 1.9 b.y. ago—Nd isotopic evidence from the basement of the North-American mid-continent. Geol. Soc. Am. Bull. 96 (6), 746–754.

Nimis, P., Taylor, W.R., 2000. Single clinopyroxene thermobarometry for garnet peridotites: Part 1. Calibration and testing of a Cr-in-Cpx barometer and an enstatite-in-Cpx thermometer. Contrib. Mineral. Petrol. 139, 541–554.

O'Neill, H.S.C., Wood, B.J., 1979. An empirical study of Fe–Mg partitioning between garnet and olivine and its calibration as a geothermometer. Contrib. Mineral. Petrol. 70, 59–70.

O'Reilly, S.Y., Griffin, W.L., 1985. A xenolith-derived geotherm for southeastern Australia and its geophysical implications. Tectonophys 111, 41–63.

O'Reilly, S.Y., Griffin, W.L., 1996. 4-D lithosphere mapping: a review of the methodology with examples. Tectonophysics 262, 3–18.

O'Reilly, S.Y., et al., 2001. Proc. Slave–Kaapvaal Workshop, Merrickville, Canada, Sept. 5–9, 2001. www.cg.nrcan.gc.ca/slave–kaapvaal-workshop/2001.

Osipova, I.L., Hjelt, S.-E., Vanyan, L.L., 1989. Source field problems in northern parts of the Baltic Shield. Phys. Earth Planet. Int. 53, 337–342.

Patchett, P.J., Arndt, N.T., 1986. Nd isotopes and tectonics of 1.9–1.7 Ga crustal genesis. Earth Planet. Sci. Lett. 78 (4), 329–338.

Pearson, D.G., 1999. The age of continental roots. Lithos 48, 171–194.

Pearson, D.G., Boyd, F.R., Hoal, K.E.O., Hoal, B.G., Nixon, P.H., Rogers, N.W., 1994. A Re–Os isotopic and petrological study of Namibian peridotites; contrasting petrogenesis and composition of on- and off-craton lithospheric mantle. Mineral. Mag. 58A (L–Z), 703–704.

Pearson, D.G., Shirey, S.B., Harris, J.W., et al., 1998. Sulphide inclusions in diamonds from the Koffiefontein kimberlite, S Africa: constraints on diamond ages and mantle Re–Os systematics. Earth Planet Sci. Lett. 160 (3–4), 311–326.

Pearson, D.G., Shirey, S.B., Bulanova, G.P., et al., 1999. Re–Os isotope measurements of single sulfide inclusions in a Siberian diamond and its nitrogen aggregation systematics. Geochim. Cosmochim. Acta 63 (5), 703–711.

Petersen, N., Bleil, U., 1982. Magnetic properties of rocks. In: Angenheister, G. (Ed.), Landolt–Börnstein: Numerical Data and Functional Relationships in Science and Technology. Springer-Verlag, Berlin, pp. 366–432.

Petit, C., Ebinger, C., 2000. Flexure and mechanical behavior of cratonic lithosphere; gravity models of the East African and Baikal rifts. J. Geophys. Res. 105, 19151–19162.

Pilkington, M., 1991. Mapping elastic lithospheric thickness variations in Canada. Tectonophys 190, 283–297.

Pizzolato, L., Schultze, D.J., 2003. Geochemistry of peridotites and eclogites from the Kelsey Lake kimberlite, Colorado–Wyoming, USA. Proc. 8th Intern. Kimberlite Conf., Victoria, BC, Canada, June 2003: FLA-0300.

Pokhilenko, N.P., Pearson, D.G., Boyd, F.R., and Sobolev, N.V., 1991. Megacrystalline dunites and peridotites: hosts for Siberian diamonds. Ann. Rep. Dir. Geophys. Lab., Carnegie Inst., Washington, 1990–1991: 11–18.

Pollack, H.N., 1986. Cratonization and thermal evolution of the mantle. Earth Planet. Sci. Lett. 80, 175–182.

Pollack, H.N., Chapman, D.S., 1977. On the regional variation of heat flow, geotherms, and lithospheric thickness. Tectonophysics 38, 279–296.

Pollack, H.N., Hurter, S.J., Johnson, J.R., 1993. Heat flow from the Earth's interior: analysis of the global data set. Rev. Geophys. 31, 267–280.

Poudjom Djomani, Y.H., Fairhead, J.D., Griffin, W.L., 1999. The flexural rigidity of Fennoscandia: reflection of the tectonothermal age of the lithospheric mantle. Earth Planet Sci. Lett. 174, 139–154.

Poupinet, G., Arndt, N., Vacher, P., 2003. Seismic tomography beneath stable tectonic regions and the origin and composition of the continental lithospheric mantle. Earth Planet. Sci. Lett. 212, 89–101.

Preston, R.F., Sweeney, R.J., 2003. A comparison of clinopyroxene thermobarometric techniques: applied to Jwaneng, Orapa and Markt kimberlites. Proc. 8th Intern. Kimberlite Conf., Victoria, BC, Canada, June 2003: FLA-0053.

Read, G.H., Grutter, H.S., Winter, L.D.S., Luckman, N.B., Gaunt, G.F. M., 2003. Stratigraphic relations, kimberlite emplacement and lithospheric thermal evolution, Quiricó Basin, Minas Gerais State, Brazil. Proc. 8th Intern. Kimberlite Conf., Victoria, BC, Canada, June 2003.

Reymer, A.P.S., Schubert, G., 1987. Phanerozoic and Precambrian crustal growth. In: Kröner, A. (Ed.), Proterozoic Lithospheric Evolution AGU, Geodyn. Ser., vol. 17, pp. 1–9.

Ritsema, J., van Heijst, H., 2000. New seismic model of the upper mantle beneath Africa. Geology 28 (1), 63–68.

Rudnick, R.L., 1995. Making continental crust. Nature 378, 571–578.

Rudnick, L.R., Nyblade, A.A., 1999. The thickness and heat production of Archean lithosphere: constraints from xenolith thermobarometry and surface heat flow. In: Fei, Y., Bertka, C.M., Mysen, B.O. (Eds.), Mantle Petrology: Field Observations and High Pressure Experimentation: A Tribute to Francis R. (Joe). Boyd. Chem. Soc. Spec., vol. 6.

Rudnick, L.R., McDonough, W.F., O'Connel, R.J., 1998. Thermal structure, thickness and composition of continental lithosphere. Chem. Geol. 145, 395–411.

Ryan, C.G., Griffin, W.L., Pearson, N.J., 1996. Garnet geotherms: pressure–temperature data from Cr-pyrope garnet xenocrysts in volcanic rocks. J. Geophys. Res. 101, 5,611–5,625.

Safonov, A.S., Bubnov, V.M., Sysoev, B.K., Chernyavsky, G.A., Chinareva, O.M., Shaporev, V.A., 1976. Deep magnetotelluric surveys of the Tungus Syneclise and on the West Siberian Plate. In: Adam, A. (Ed.), Geoelectric and Geothermal Studies. Akad. Kiado, Budapest, Hungary, pp. 666–672.

Schmidberger, S.S., Francis, D., 1999. Nature of the mantle root beneath the North American craton: mantle xenolith evidence from Somerset Island kimberlites. Lithos 48, 195–216.

Schultz, A., Kurtz, R.D., Chave, A.D., Jones, A.G., 1993. Conductivity discontinuities in the upper mantle beneath a stable craton. Geophys. Res. Lett. 20, 2941–2944.

Shankland, T.J., Duba, A.G., 1990. Standard electrical conductivity of isotropic, homogenous olivine in the temperature range 1200–1500 °C. Geophys. J. Int. 103, 25–31.

Shapiro, N.M., Ritzwoller, M.H., 2004a. Thermodynamic constraints on seismic inversions. Geophys. J. Int. doi:10.1111/j.1365-246X.2004.02254.x.

Shapiro, N.M., Ritzwoller, M.H., 2004b. Inferring surface heat flux distributions guided by a global seismic model: particular application to Antarctica. Earth Planet Sci. Lett. 223, 213–224.

Simons, F.J., Zuber, M.T., Korenaga, J., 2000. Isostatic response of the Australian lithosphere: estimation of effective elastic thickness and anisotropy using multitaper spectral analysis. J. Geophys. Res. 105, 19163–19184.

Simpson, F., 2002. A comparison of electromagnetic distortion and resolution of upper mantle conductivities beneath continental Europe and the Mediterranean using islands as windows. Phys. Earth Planet. Int. 129, 117–130.

Singh, R.P., Kant, Y., Vanyan, L., 1995. Deep electrical conductivity structure beneath the southern part of the Indo-Gangetic plains. Phys. Earth Planet. Int. 88, 273–283.

Sleep, N.H., 2003. Geodynamic implications of xenolith geotherms. Geochem. Geophys. Geosyst. 4 (9), 1079. doi:10.1029/ 2003GC000511.

Smith, D., 1999. Temperatures and pressures of mineral equilibration in peridotite xenoliths: review, discussion, and implications. In: Fei, Y., Bertka, C.M., Mysen, B.O. (Eds.), Mantle Petrology: Field Observations and High Pressure Experimentation: a Tribute to Francis R. (Joe). Boyd. Spec. Publ. Geochemical Soc., vol. 6, pp. 171–188.

Sobolev, S.V., Zeyen, H., Stoll, G., Werling, F., Altherr, R., Fuchs, K., 1996. Upper mantle temperatures from teleseismic tomography of French Massif Central including effects of composition, mineral reactions, anharmonicity, anelasticity and partial melt. Earth Planet. Sci. Lett. 139, 147–163.

Spakman, W., 1990. The structure of the lithosphere and mantle beneath the Alps as mapped by delay time tomography. In: Freeman, R., Giese, P., Mueller, St. (Eds.), The European Geotraverse: Integrative Studies. ESF, Strasbourg, pp. 213–220.

Tilmann, F., Ni, J., INDEPTH III Seismic Team, 2003. Seismic imaging of the downwelling Indian lithosphere beneath central Tibet. Science 300 (5624), 1424–1427.

Vanyan, L.L., Cox, C.S., 1983. Comparison of deep conductivities beneath continents and oceans. J. Geomagn. Geoelectr. 35 (11-1), 805–809.

Vanyan, L.L., Berdichewski, M.N., Fainberg, E.B., 1977. Study of asthenosphere of East European platform by electromagnetic sounding. Phys. Earth Planet. Int. 14 (2), P1–P2.

Wang, Y., Mareschal, J.-C., 1999. Elastic thickness of the lithosphere in the central Canadian Shield. Geophys. Res. Lett. 26, 3033–3036.

Watts, A.B., 2001. Isostasy and Flexure of the Lithosphere. Cambridge Univ. Press. 458 pp.

Watts, A.B., Lamb, S.H., Fairhead, J.D., Dewey, J.F., 1995. Lithospheric flexure and bending of the central Andes. Earth Planet. Sci. Lett. 134 (1–2), 9–21.

Windley, B.F., 1995. The Evolving Continents. John Wiley and Sons, Chichester, New York. 489 pp.

Wu, X., Ferguson, I.J., Jones, A.G., 2002. Magnetotelluric response and geoelectric structure of the Great Slave Lake shear zone. Earth Planet. Sci. Lett. 196, 35–50.

Xu, X., O'Reilly, S.Y., Zhou, X., Griffin, W.L., 1996. A xenolith-derived geotherm and the crust–mantle boundary at Qilin, southeastern China. Lithos 38, 41–62.

Xu, X., O'Reilly, S.Y., Griffin, W.L., Zhou, X., 2000. Genesis of young lithospheric mantle in southeastern China; an LAM-ICPMS trace element study. J. Petrol. 41, 111–148.

Zhdanov, M.S., Golubev, N.G., Varentsov, I.M., 1986. 2-D model-fitting of a geomagnetic anomaly in the Soviet Carpathians. Ann. Geophys. Ser., B 4 (3), 335–341.